Université de Sherbrooke

# Mesure par spectroscopie des pertes d'énergie de la section efficace des dommages causés par l'impact des électrons de basse énergie sur des films solides de $CO_2$ et de cyclopropane

par

Mathieu C. DESCHAMPS

Département de radiobiologie et médecine nucléaire

Mémoire présenté à la Faculté de médecine
en vue de l'obtention du grade de
Maître ès sciences (M.Sc.) en radiobiologie

Juillet 2003

*Your file Votre référence*
*ISBN: 0-612-90595-0*
*Our file Notre référence*
*ISBN: 0-612-90595-0*

RÉSUMÉ

# MESURE PAR SPECTROSCOPIE DES PERTES D'ÉNERGIE DE LA SECTION EFFICACE DES DOMMAGES CAUSÉS PAR L'IMPACT DES ÉLECTRONS DE BASSE ÉNERGIE SUR DES FILMS SOLIDES DE $CO_2$ ET DE CYCLOPROPANE

Mathieu C. DESCHAMPS

Mémoire présenté à la Faculté de médecine en vue de l'obtention du grade de Maître ès sciences (M.Sc.) en radiobiologie

Département de radiobiologie et médecine nucléaire, Faculté de médecine, Université de Sherbrooke, Sherbrooke, Québec, Canada

Le passage de la radiation ionisante dans la matière libère un grand nombre d'électrons de basse énergie (0-50 eV). À ces énergies, l'étude des sections efficaces de diffusion des électrons sur les atomes et les molécules est importante étant donné la formation d'ions négatifs transitoires, c'est-à-dire de résonances d'électrons, qui entraînent des modulations considérables dans ces sections efficaces. De plus, les électrons de basse énergie interagissent efficacement avec le milieu irradié où ils provoquent des bris moléculaires et peuvent produire des espèces chimiques réactives.

Nous avons premièrement étudié l'interaction des électrons de basse énergie avec des films minces de $CO_2$ condensés sur un substrat d'argon solide. Nous avons alors constaté que la molécule de $CO_2$ peut se fragmenter et produire du CO suite à l'interaction avec ces électrons. Nous avons ici mesuré la section efficace absolue pour cette production de CO. Le fragment de CO qui demeure piégé dans le film de $CO_2$ est détecté *in situ* par spectroscopie électronique par pertes d'énergie via son premier état électronique $d^3\Pi$. La production de CO est mesurée avec un bombardement constant pour différentes énergies des électrons sur la plage d'énergie de 1 à 30 eV. Cette plage correspond à l'énergie où la majorité des électrons secondaires sont créés lors de l'irradiation d'un système. Nous

rapportons également le spectre des pertes d'énergie pour les transitions électroniques de ces mêmes films de $CO_2$. Ce dernier spectre a été obtenu avec une acquisition de courte durée (petite exposition) afin de minimiser l'influence de la production de CO et permet d'identifier les états neutres excités et le premier état ionique de la molécule de $CO_2$. Les variations dans la production de CO en fonction de l'énergie des électrons sont interprétées par la formation d'ions négatifs transitoires (résonances). Ces ions transitoires peuvent mener directement à la fragmentation de la molécule par attachement dissociatif ou indirectement en décroissant dans une région répulsive d'un état neutre excité ou dans une région répulsive d'un état de l'ion positif.

Deuxièmement, nous avons étudié les réactions induites par des électrons de basse énergie dans des films minces de cyclopropane. Les produits de réaction sont identifiés à l'aide des altérations engendrées dans les spectres de vibrations et de transitions électroniques de l'échantillon. Le propène est identifié comme étant le produit initial majoritaire mais la formation de chaînes moléculaires plus longues est également observée. Ces résultats montrent donc non seulement que les électrons de basse énergie peuvent mener à une fragmentation moléculaire mais aussi induire des liens chimiques et donc mener à la formation de molécules plus complexes. Nous avons également mesuré la section efficace de production de propène dans ces films de cyclopropane et étudié cette production en fonction de l'épaisseur de l'échantillon et de l'épaisseur du substrat d'argon séparant l'échantillon du support de platine.

Mots clés : électrons, résonances, dissociation, $CO_2$, cyclopropane

*AVANT-PROPOS*

Le présent mémoire regroupe quatre articles comprenant la majeure partie de mes travaux réalisés au cours de mon inscription au programme de *maîtrise en radiobiologie.* Les deux premiers articles portent sur le dioxyde de carbone et résultent de mon travail expérimental. La rédaction de ces deux premiers articles fut sous ma responsabilité avec le soutien de M. Marc Michaud. Les deux derniers articles portent quant à eux sur le cyclopropane. Les résultats expérimentaux proviennent de mon travail en collaboration avec la Dre Petra Swiderek. La phase de rédaction des articles sur le cyclopropane fut toutefois prise en charge par Dre Swiderek, ma participation se limitant alors à des discussions et commentaires.

TABLE DES MATIÈRES

Listes des Tables et figures

LISTE DES SIGLES, ABRÉVIATIONS ET SYMBOLES

| | |
|---|---|
| CP | Cyclopropane ($C_3H_6$) |
| DEA | Attachement dissociatif d'électron (Dissociative Electron Attachment). |
| $E_0$ | Énergie incidente des électrons. |
| eV | Électron-volt ( = $1.6 \times 10^{-19}$ joule);<br>meV ($10^{-3}$ eV); keV ($10^3$ eV); MeV ($10^6$ eV). |
| EBE | Électron(s) de basse énergie |
| EEL | Énergie perdue des electrons (Electron Energy Loss). |
| FWHM | Pleine largeur à mi-hauteur (Full Width at Half Maximum). |
| HREEL | Mesure des pertes d'énergie des electrons à haute resolution (High Resolution Electron Energy Loss). |
| HREELS | Spectromètre (ou spectroscopie) d'électrons par pertes d'énergie à haute résolution. |
| $I_0$ | Courant d'électrons incident sur la cible |
| $S_0$ | Surface du faisceau d'électrons à la cible |
| $\sigma_p$ | Section efficace de production d'un fragment |
| $\theta_0$ | Angle d'incidence du faisceau d'électrons par rapport à la normale de la cible. |
| $\theta_S$ | Angle de détection du faisceau d'électrons diffusé par rapport à la normale de la cible. |
| UHV | Hyper-vide (Ultra High Vacuum) |

# I. INTRODUCTION

La radiobiologie a pour but d'étudier les interactions des radiations ionisantes avec la matière biologique ainsi que les effets de ces interactions sur les mécanismes biologiques. On divise généralement la radiobiologie en quatre grandes étapes. Premièrement, l'étape physique consiste au passage de la radiation ionisante dans le milieu créant une succession d'ionisations. Un grand nombre d'électrons de basse énergie (EBE) sont produits à cette étape. Deuxièmement, lors de l'étape physico-chimique, les EBE interagissent avec les molécules du milieu en formant notamment des ions négatifs transitoires (*i.e.*, des résonances). Ces interactions peuvent mener à la fragmentation moléculaire et à la production d'ions et de radicaux libres. Troisièmement, on distingue l'étape chimique où les fragments et radicaux produits à l'étape précédente réagissent avec leur environnement induisant une ou des réactions chimiques. Finalement, arrive l'étape biologique où la cellule répond aux modifications chimiques induites. Cette réponse peut mener à des effets mutagènes et cancérigènes ou tout simplement à la mort cellulaire.

Les recherches exposées dans le présent mémoire ont pour but d'amener des informations supplémentaires afin de mieux comprendre l'étape physico-chimique de la radiobiologie. En effet, nous avons étudié l'interaction d'électrons de basse énergie (< 30 eV) avec des molécules simples telles que le dioxyde de carbone ($CO_2$) et le cyclopropane ($C_3H_6$). L'emphase fut surtout mise sur la dissociation de ces molécules et sur la mesure des sections efficaces de production d'un fragment neutre précis lors de la dissociation. L'étude de ces molécules est précieuse afin de pouvoir interpréter les phénomènes impliqués dans l'interaction des EBE avec des molécules plus complexes telles que des

protéines ou l'ADN. De plus, le dioxyde de carbone est reconnu pour jouer un rôle important dans la chimie des atmosphères de Mars, Venus et la Terre, en plus d'être impliqué dans le réchauffement planétaire et dans les mécanismes de respiration. De son côté, la molécule de cyclopropane présente un intérêt considérable étant donné qu'il s'agit du plus petit cycle d'hydrocarbures et qu'en ce sens son étude servira de précurseur pour les cycles plus importants pour la biologie.

Nous présentons ici deux articles portant sur le dioxyde de carbone ainsi que deux articles sur le cyclopropane. Le premier article sur le dioxyde de carbone s'intéresse particulièrement à l'étude des états électroniques du $CO_2$ en phase condensée. Des modifications importantes entre la phase gazeuse et la phase condensée y sont rapportées. Le deuxième article présente la mesure des sections efficaces pour la production de monoxyde de carbone (CO) due à l'impact de EBE entre 2 et 30 eV sur du $CO_2$ en phase condensée. Le troisième article porte sur l'identification des produits résultants de l'irradiation de films de cyclopropane par des EBE. Le propène ($CH_2$-CH-$CH_3$) est identifié comme étant le produit initial majeur mais la formation de chaînes moléculaires plus longues est également constatée. Cet article montre donc que les EBE peuvent non seulement induire des bris moléculaires mais aussi initier des réactions chimiques menant à la formation de molécules plus complexes. Le dernier des quatre articles présente les sections efficaces pour la production de propène suite à l'irradiation de films de cyclopropane par des électrons de 15 eV.

Il est à noter que les méthodes expérimentales et les discussions sur les résultats sont inclus à même les articles. Toutefois, une conclusion générale est présentée à la fin de l'ouvrage afin de mettre les travaux dans une perspective plus globale. Néanmoins, avant

de présenter chacun de ces articles, expliquons pourquoi les EBE jouent un rôle important en radiobiologie et comment ces électrons mènent à la dissociation moléculaire de façon efficace.

## I.1. POURQUOI ÉTUDIER LES ÉLECTRONS DE BASSE ÉNERGIE EN RADIOBIOLOGIE.

Bien que par définition une radiation ionisante possède tout juste suffisamment d'énergie pour ioniser une molécule, l'usage commun du terme suggère plutôt une radiation de haute énergie. On parle souvent de radiations ayant une énergie de plusieurs keV jusqu'à quelques MeV. Ces radiations de haute énergie interagissent avec la matière principalement par un processus d'ionisation, perdant un peu d'énergie à chaque ionisation et produisant des électrons secondaires. On estime généralement qu'un rayon $\beta^-$ de 1 MeV produit sur son passage jusqu'à 30 000 électrons secondaires ayant une énergie inférieure à 100 eV. Ce sont ces électrons secondaires que nous appelons électrons de basse énergie (EBE). Notre attention se portera cependant surtout sur des électrons ayant une énergie inférieure à 30 eV.

Les électrons secondaires ont longtemps été négligés dans l'élaboration de simulations reproduisant les dommages induits suite au passage d'une radiation de haute énergie. Or, ces électrons possèdent encore une quantité d'énergie bien suffisante pour induire des dommages. Par exemple, les EBE peuvent induire des cassures double-brins de l'ADN [Boudaïffa B. *et al.*, 2000]. Ainsi, leur présence en grand nombre et dans des régions localisées fait en sorte qu'ils ne peuvent être négligés. Or, le mode d'interaction des électrons se complexifie à basse énergie étant donné la possibilité de former des résonances. Il est donc essentiel de comprendre l'interaction des électrons de basse énergie avec la matière et surtout de mesurer les sections efficaces avec lesquelles certains

processus surviennent afin de développer de meilleures simulations pour la radiobiologie et aboutir à une meilleure compréhension des dommages causés par le passage d'une radiation ionisante.

## I.2. INTERACTION DES ÉLECTRONS DE BASSE ÉNERGIE AVEC DES MOLÉCULES ET FRAGMENTATION MOLÉCULAIRE.

Les processus d'interaction entre électrons et molécules sont généralement divisés en deux catégories : résonants et non-résonants (ou directs). Les processus résonants sont initiés par l'attachement d'un électron sur un atome ou une molécule formant ainsi un ion négatif transitoire. On peut répertorier les résonances en deux classes principales. La résonance de forme (*shape resonance*), ou résonance à une particule, consiste en l'attachement d'un électron par la barrière de potentiel créée par le moment cinétique d'une molécule. D'autre part, la résonance à cœur excité (*core-excited resonance*), ou résonance à un trou et deux particules, survient lorsque l'électron incident cède une partie de son énergie afin de promouvoir un électron de la molécule vers une orbitale libre et que l'électron incident s'attache à cette orbitale. Ainsi, l'ion transitoire formé par une résonance peut se trouver dans un état fondamental ou excité.

Une résonance peut évoluer selon différents canaux de décroissance tel que montré à la figure 1 pour une molécule diatomique [Sanche L., 1995]. D'abord, l'électron peut s'autodétacher tout en laissant la molécule dans un état vibrationnel ou électronique excité (1). Si cet état excité est dissociatif, la molécule se dissociera en fragments neutres (2). Lorsque le temps de vie de la résonance est suffisamment long et que l'ion négatif transitoire est dissociatif dans la région de Franck-Condon, un ou des fragments neutres et un fragment chargé négativement peuvent être formés (3 et 4). On parle alors

d'attachement dissociatif (DEA, pour *dissociative electron attachment*). L'ion transitoire peut également se stabiliser en transférant un surplus d'énergie au milieu environnant (5). Finalement, si la résonance possède une énergie supérieure au potentiel d'ionisation de la molécule, l'émission de deux électrons est possible (6). Dans le cas où l'ion positif ainsi formé est instable, la molécule se dissociera.

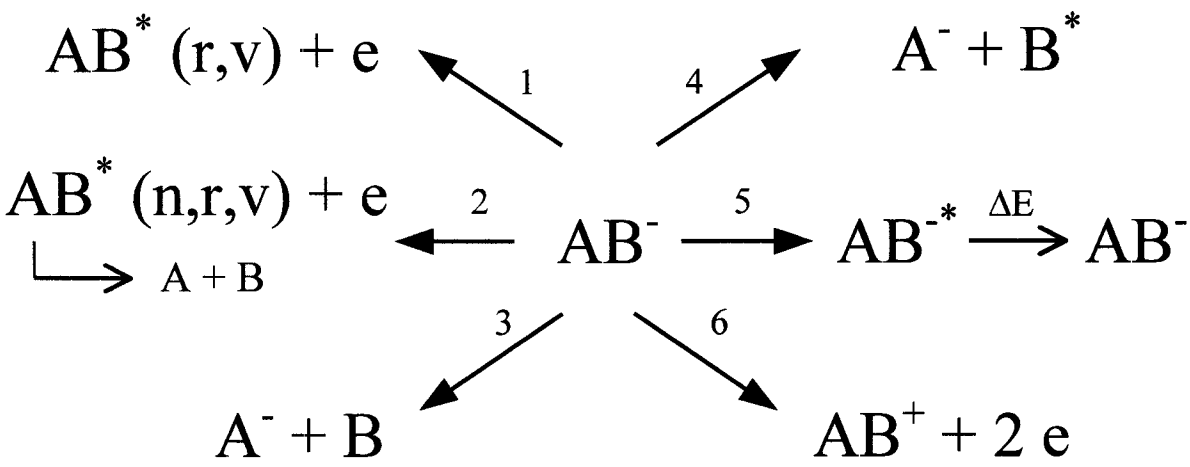


Fig.1 Canaux de décroissance d'une résonance pour une molécule diatomique.

La formation d'une résonance présente donc de nombreux canaux de décroissance pouvant mener à la dissociation moléculaire. De plus, étant donné que dans un processus résonant l'électron réside dans l'entourage de la molécule pour un temps beaucoup plus long que pour un processus direct, les transferts d'énergie sont favorisés. Ainsi, la présence d'une résonance affecte considérablement les sections efficaces menant à une excitation vibrationnelle ou électronique ou conduisant à la dissociation moléculaire. Les processus directs, favorisés à plus haute énergie, montrent généralement peu de dépendance ou une très lente variation avec l'énergie incidente. De ces faits, l'étude de l'impact des EBE sur des molécules présente un intérêt afin d'identifier et de quantifier les mécanismes résonants pouvant notamment mener à la fragmentation moléculaire.

# II. RÉSULTATS

## II.1. ARTICLE no 1 : Low-energy electron-energy-loss spectroscopy of electronic transitions in solid carbon dioxide

# Low-energy electron-energy-loss spectroscopy of electronic transitions in solid carbon dioxide

**M. C. Deschamps, M. Michaud, and L. Sanche**[†]

Groupe des Instituts de Recherche en Santé du Canada en Sciences des Radiations, Université de Sherbrooke, Sherbrooke, Québec, Canada J1H 5N4

## Abstract

We report electron-energy-loss spectra of solid films of $CO_2$ for electronic transitions induced by 15, 19.4 and 25 eV incident electrons. All spectra were obtained under sufficiently small electron exposures so as to avoid sample damages. The use of low-energy electron along with the backscattering geometry gives access to spin- and symmetry-forbidden transitions while the effect of the condensed phase makes it possible to modify the energy, ordering and magnitude of most gas-phase transitions. The most noticeable observation is the disappearance of all sharp energy-loss peaks attributed to Rydberg series of $CO_2$ in the gas phase. In contrast, transitions to the molecular valence $^{3,1}\Delta_u$ and $^{3,1}\Sigma_u^-$ states are located virtually at the same energy as in the gas phase. The strong electric dipole allowed valence $^1\Sigma_u^+$ transition is found shifted to lower energy by about 0.3 eV while transitions to mixed Rydberg-valence $^{3,1}\Pi_g$ and $^1\Pi_u$ states are both shifted to higher energy by about 0.4 - 0.5 eV. The lowest valence $^3\Sigma_u^+$ transition is ascribed to the lowest energy-loss feature in the solid at 7.9 eV.

KEYWORDS: carbon dioxide, electronic, condensed phase, electron

[†]Canada Research Chair in the Radiation Sciences

## I. INTRODUCTION

Electronic states of carbon dioxide molecules ($CO_2$) have been studied both experimentally and theoretically owing to their fundamental interest and practical applications. Several electron impact experiments ranging from threshold up to 100 eV of incident energy[1-6] and optical absorption[7, 8] experiments have been devoted to study low-lying electronic states of $CO_2$. Many *ab-initio* calculations of its electronic structure, several of which pertain to the linear geometry only, have been performed using different methods at various levels of approximation.[9-18] In general, it is predicted that most of the valence states of $CO_2$ are bent whereas the Rydberg states are linear.

The presence of both linear and bent geometry in the electronic excitation of $CO_2$ leads to difficulties in the analysis of the experimental spectra and necessitates calculations of the energy of the states as a function of the bending angles. The complications arise essentially from the crossing and avoided crossing of the potential energy function of these electronic states upon changes in the bending angles. Seven electronic states, $^3\Sigma_u^+$, $^{3,1}\Sigma_u^-$, $^{3,1}\Delta_u$ and $^{3,1}\Pi_g$, are believed to lie between 7 and 10 eV of excitation energy. Early theoretical[9] and experimental[1] studies of this energy region showed a general agreement. However, the assignment of the electronic transitions in this region of the spectrum remains complicated owing to overlapping of the experimental features and disagreements among the ordering of the states as shown in more recent calculations.[12, 15, 16, 18] Above 10 eV, the excitation spectrum is composed of several Rydberg series and Rathenau progressions.[3, 4] Among these, transitions to the $^1\Sigma_u^+$ state and $^1\Pi_g$ state are usually identified at 11.04 eV and 11.4 eV respectively. While for most

of these states their Rydberg character has been confirmed experimentally, the same is not true for the $^1\Sigma_u^+$ state, as some experimental results seem to give a valence character to this state.[3, 7] Most of the electron-energy-loss (EEL) spectra reported to date have been carried out in the gas phase and no EEL experiment has been reported for electronic transitions in the condensed phase.

Our aim in the present article is to provide new information from the solid phase to help understanding further the electronic structure of $CO_2$. Owing to the backscattering geometry and low incident energies at which the present EEL spectra are recorded, our results are more sensitive to symmetry- and spin-forbidden transitions. Also, the avoided crossing due to the particular ordering of the electronic states of the molecule is not expected to take place in the solid phase owing to the upward energy shift suffered generally by Rydberg states upon condensation. Thus, by modifying the character and energy of some electronic transitions, the present experiment provides an additional insight in the assignment of specific electronic states.

## II. EXPERIMENT

The electron-scattering measurements were performed with a high-resolution electron-energy-loss spectrometer consisting of two hemispherical deflectors (*i.e.*, monochromator and analyzer), as described in detail previously.[19] The angle of incidence $\theta_0$ can be varied between 8° and 80° from the normal to the sample. The angle of analysis $\theta_d$ is fixed at 45° at the opposite azimuth. Double-zoom electron lenses at the exit of the monochromator and at the entrance of the analyzer allow constant focusing and beam size

over a wide incident energy range (*e.g.*, 2 – 25 eV) along with minimum variations of the instrument transmission. The apparatus is housed in a μ-metal UHV chamber maintained at a base pressure of 1 x $10^{-10}$ Torr by an ion pump and a liquid-$N_2$ cooled titanium sublimation pump. In the present experiment, the combined resolution of the selectors was set at 15 meV full width at half maximum (FWHM) for a current of 0.2 nA at the substrate. The incident electron energy $E_0$ was calibrated within ±0.1 eV with respect to the vacuum level by measuring the threshold of the electron current transmitted through the samples.

The samples are initially prepared in a gas-handling manifold that consists of two gas or vapor sources connected through bypass and precision-leak valves to a small calibrated volume. The absolute pressure in this volume is measured with a capacitance manometer. For each deposited sample, a known amount of gas or vapor, which is measured by the differential pressure drop in the calibrated volume, is leaked via a stainless steel capillary whose end is located just in front of a Pt(111) single crystal. The crystal is mounted on a sample manipulator,[20] which allows azimuthal rotation, flip and X, Y and Z translations of the sample. The crystal is held at a temperature of 18 K via a flexible copper braid attached to the cold head of a close-cycle helium refrigerator (APD Cryogenics Inc. Allentown, PA). Crystal cleaning is achieved by resistive heating at 1100 K and sequences of $Ar^+$ sputtering followed by annealing and heating in the presence of oxygen at about 900 K.

Carbon dioxide gas was supplied by Matheson of Canada Ltd. with a stated purity of 99.9995 %. The number of condensed layers of $CO_2$ was estimated to ± 20 % from the calibrated amount of gas needed to deposit a monolayer, assuming no change of the

sticking coefficient and growth mode for the adlayers, as described previously.[21] Carbon dioxide gas is known to condense between 10 and 30 K as a metastable amorphous solid film that transforms irreversibly to the crystalline form upon annealing to 50 – 77 K.[22] The absence of a strong electron elastic reflectivity in the specular direction (i.e., the elastic reflectivity at $\theta_0 = 45^\circ$ being similar to that at $\theta_0 = 8^\circ$ ) indicated that our films consisted primarily of randomly oriented crystallites and/or amorphous material.

Measurements that exhibited slight sample charging and/or decomposition were rejected by comparing the transmitted current onset and EEL spectra at different time intervals. Long electron exposures lead to sample damages for all electron impact energies used here. More particularly, evidences were found for molecular fragmentation leading to the production of CO molecules that remain confined in the $CO_2$ films. This phenomenon, which will be disclosed in more details in a forthcoming publication,[23] had to be taken into account during our measurements. More specifically, all spectra in the present work were obtained under sufficiently small electron exposures (i.e. short acquisition times) in order to make the contribution from CO negligible. In practice, this was achieved by limiting the acquisition time to less than six minutes for an electron beam current of 0.2 nA incident on a same film location. Then the sample was translated in X and/or Y directions so as to probe a new spot on the film. The number of such acquisitions was limited to ten different locations on the same film, after which a fresh film was deposited.

## III. RESULTS AND DISCUSSION

The carbon dioxide molecule is a linear triatomic molecule with 16 valence electrons. The molecule in the ground state belong to the $D_{\infty h}$ point group with the electronic configuration $...(3\sigma_g)^2(2\sigma_u)^2(4\sigma_g)^2(3\sigma_u)^2(1\pi_u)^4(1\pi_g)^4(2\pi_u^*)^0(5\sigma_g^*)^0(4\sigma_u^*)^0...$, $X^1\Sigma_g^+$. Drawings of these molecular orbitals (MO's) can be found in the Jorgensen and Salem book.[24] The promotion of a $1\pi_g$ electron into the first unoccupied orbital $2\pi_u$ gives rise to six electronic states in the linear geometry ($^{3,1}\Sigma_u^+$, $^{3,1}\Sigma_u^-$, and $^{3,1}\Delta_u$). Except for the $^1\Sigma_u^+$ state, which is computed to lie further above the others and to have some Rydberg character (i.e., $1\pi_g \rightarrow 3p\pi_u$),[9, 18] transitions from the ground state to these excited states are classified as valence excitations. States of $^{3,1}\Pi_g$ and $^{3,1}\Pi_u$ symmetries arise from the promotion of a $1\pi_g$ electron into the $3s\sigma_g$ and $3p\sigma_u$ orbitals, respectively. The $^{3,1}\Pi_g$ states have a Rydberg or mixed Rydberg-valence character, whereas $^{3,1}\Pi_u$ states are essentially of the Rydberg type (Table I).

The electronic EEL spectrum of a 15-layer solid film of $CO_2$ condensed on Pt(111) is shown in Fig. 1(a) for three different incident energies $E_0$ = 15, 19.4, and 25 eV. The angle of incidence $\theta_0$ is 15° and that of analysis $\theta_d$ is 45°. The 19.4-eV spectrum is a compilation of 50 acquisitions of two minutes. Those at 15 and 25 eV are each a compilation of ten acquisitions of six minutes. It should be mentioned that at larger incident angles (i.e., $\theta_0$ = 30°, 45° and 60°) no significant change was observed in the spectra. In Fig. 1(b) we show the 19.4-eV spectrum subtracted from the mean curved line (i.e., obtained by adjacent averaging) and amplified to enhance the visibility of the structures. The present energies and assignments are tabulated along with EEL

measurements in the gas phase and optical results in both the gas and solid phase in Table II.

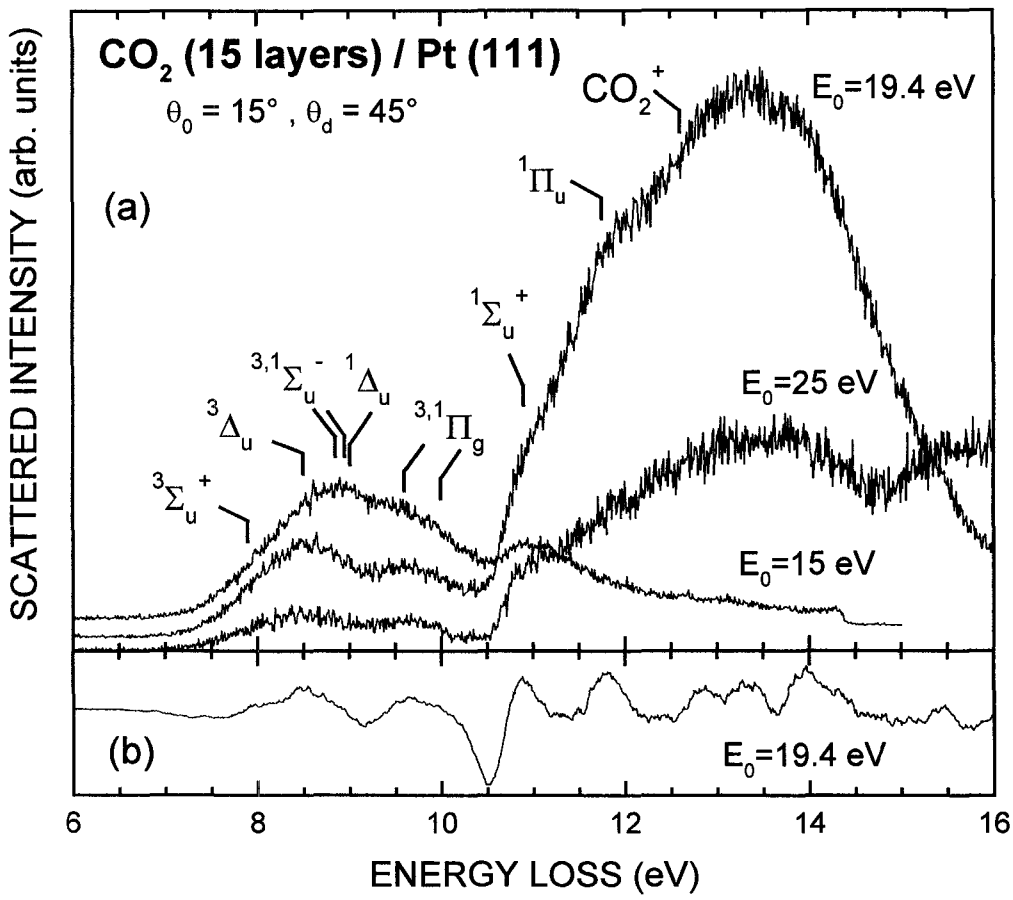


Fig. 1. (a) Electronic EEL spectra for 15 eV, 19.4 eV and 25 eV electrons incident on a 15-layer solid film of $CO_2$ condensed on Pt(111). The labels assigned to the electronic energy losses are discussed in the text. Each spectrum is a collection of acquisitions obtained under small electron exposure (i.e. short acquisition times) so as to make sample damage negligible. (b) The 19.4-eV spectrum subtracted from the mean curved line obtained by adjacent averaging and amplified to enhance the visibility of the structures.

Table I. Calculated vertical excitation energies for $CO_2$ (in eV)

| States | Winter[a] | England[b] | Nakatsuji[c] | Spielfiedel[d] | Lee[e] | Buenker[f] |
|---|---|---|---|---|---|---|
| $^3\Sigma_u^+$ | 7.35 | 8.65 | 8.04 | 8.35 | 8.53 | |
| $^3\Delta_u$ | 7.83 | 9.02 | 8.67 | 8.83 | 9.13 | |
| $^3\Sigma_u^-$ | 8.24 | 9.42 | 9.05 | 9.21 | 9.73 | |
| $^1\Sigma_u^-$ | 8.27 | 9.42 | 9.13 | 9.19 | 9.73 | 9.42 |
| $^1\Delta_u$ | 8.38 | 9.43 | 9.25 | 9.28 | 9.95 | 9.54 |
| $^3\Pi_g$ | 8.95 | 8.86 | 8.73 | 8.61 | | |
| $^1\Pi_g$ | 9.23 | 9.10 | 8.93 | 9.00 | | 9.16 |
| $^1\Sigma_u^+$ | 11.07 | 11.20 | 11.00 | | | 11.38 |
| $^3\Pi_u$ | 11.49 | 11.43 | 11.31 | | | |
| $^1\Pi_u$ | 11.53 | 11.45 | 11.39 | | | 11.64 |
| $CO_2^+ {}^2\Pi_g$ | 13.61 | | | | | |

[a] Reference 9
[b] Reference 12
[c] Reference 15
[d] Reference 16
[e] Reference 17
[f] Reference 18

From the comparison to the gas-phase electronic EEL spectra,[3, 5, 6] one can immediately see that all sharp energy-loss peaks due to the Rydberg transitions converging to the first ionization potential at 13.776 eV[25] are absent in the solid phase. Owing to the relatively large size of Rydberg orbitals compared with the closest neighbor distances in the condensed phase, the associated excitations are more susceptible to be perturbed. If the perturbations are not too severe, the Rydberg excitations are shifted slightly to higher energy, otherwise they vanish in their corresponding ionization continuum.[26] Yet these condensation effects can help to verify the Rydberg character attributed to an electronic transition in the gas phase.

Table II. Experimentally observed transition energies for $CO_2$ (in eV)

| States | Solid | | | Gas | | | | | |
|---|---|---|---|---|---|---|---|---|---|
| | Electron | Optical | | Optical | Electron | | | | |
| | This work | Monahan[a] | Abe[b] | Monahan[a] | Hall[c] | Dance[d] | McDiarmid[e] | Cvejanovic[f] | H.-F.[g] |
| $^3\Sigma_u^+$ | 7.9 | | | | ~7.3 | ~7.2 | | | |
| $^3\Delta_u$ | 8.5 | | | | ~8.1 | ~7.85 | | | |
| $^3\Sigma_u^-$ | 8.9 | | | | ~8.3 | 8.24 | | | |
| $^1\Sigma_u^-$ | 8.9 | | | | ~8.3 | 8.24 | | | |
| $^1\Delta_u$ | 8.9 | | | 8.4 | ~8.6 | 8.24 | 8.5 | | (8.5) |
| $^3\Pi_g$ | 9.6 | | | | ~8.8 | 8.24 | 8.9 ($A_2$) | 8.4 | |
| $^1\Pi_g$ | 10.0 | 9.8 | ~9.9 | 9.3 | ~9.4 | 9.25 | 9.3 ($B_2$) | | (9.3) |
| $^1\Sigma_u^+$ | 10.8 | 10.4 | 10.69 | 11.0 | | 11.0 | 11.0 | | 11.046 |
| $^3\Pi_u$ | | | | | | | | | |
| $^1\Pi_u$ | 11.75 | 11.2 | 11.7 | 11.4 | | 11.4 | 11.38 | | 11.387 |
| $CO_2^+$ $^2\Pi_g$ | 12.6 | | | | | 13.79 | 13.77 | | 13.776 |

[a] Reference 7
[b] Reference 8
[c] Reference 1
[d] Reference 2
[e] Reference 3
[f] Reference 4
[g] Reference 5

The EEL spectra at $E_0$ = 19.4 and 25 eV present between 7 and 9.1 eV a broad excitation band with a maximum at 8.5 eV along with a shallow shoulder around 7.9 eV, which can be more clearly seen with the difference spectrum in Fig. 1(b). In the 15-eV spectrum a maximum is also revealed at a slightly higher energy around 8.9 eV. For all three impact energies we observe around 9.8 eV the same broad feature that resolves almost in two excitation bands at 9.6 and 10 eV, as one can see in Fig. 1(b). At first glance, these spectral features resemble the diffused excitation bands that have been observed around 8.5 and 9.3 eV in the gas phase. Those bands are usually assigned to

the $^3\Sigma_u^+$, $^{3,1}\Sigma_u^-$ and $^{3,1}\Delta_u$ ($1\pi_g \rightarrow 2\pi_u^*$) excitations, which are known to have a valence character, and $^{3,1}\Pi_g$ ($1\pi_g \rightarrow 3s\sigma_g^*$) excitations, which have a mixed Rydberg-valence character and are predicted to be linear in their equilibrium geometry.[27] In the original calculations of the electronic structure of $CO_2$ by Winter *et al.*,[9] the $\Delta_u$ states are located at lower energy than the $\Pi_g$ states. But the opposite order is found in the later calculations of England *et al.*,[12] Nakatsuji,[15] Spielfiedel *et al.*,[16] and more recent ones of Buenker *et al.*.[18] Despite variation as to the exact ordering of these states, we note that these calculations are consistent altogether as they predict about the same small singlet-triplet splitting values of 0.2 – 0.4 eV for the $^{3,1}\Pi_g$ states and 0.4 – 0.6 eV for the $^{3,1}\Delta_u$ states. England *et al.* [12] suggested that upon bending, after the avoided crossing, the originally mixed character of the $^1\Pi_g$ state would turn into valence, whereas the valence character of the $^1\Delta_u$ and $^1\Sigma_u^-$ states would become mixed or Rydberg. As a consequence, England *et al.* [12] and Nakatsuji[15] proposed reassigning the experimental results in the gas phase so that the spectral feature at 8.5 eV would be ascribed to the $^1\Pi_g$ state, while that at 9.3 eV would be labeled as $^1\Delta_u$ state. In contrast, Buenker *et al.* [18] attributed the 9.3-eV feature to a vertical transition to the $^1\Pi_g$ state, which they computed at 9.15 eV, and the 8.5-eV feature to a non-vertical transition to an upper state correlating to the $^1\Delta_u$ state in the linear geometry, which they computed at 9.54 eV.

Among the preceding various assignments, the latter appears to be the most suitable to explain the present results. While the electronic excitation band seen around

8.5 eV in the gas phase remains virtually the same in the solid phase, the band found around 9.3 eV has disappeared. In its place, a minimum is observed along with the appearance of two excitation bands at 9.6 and 10 eV. Since there is no electronic excitation of the molecule predicted to lie within the latter energy range, this strongly suggests a shift in the energy of existing electronic states. In view of their Rydberg character in the linear geometry, transitions from the ground state to the $^{3,1}\Pi_g$ states are the most likely candidates. These states could suffer an upward energy shift of at least 0.5 eV upon condensation and since their small predicted singlet-triplet splitting both could be responsible for the present 9.6- and 10-eV energy-loss features. This also agrees with optical absorption studies of solid carbon dioxide,[7, 8] where the broad spectral feature around 9.8 eV has been ascribed to the $^1\Pi_g$ excitation. Furthermore, since the $\Pi_g$ states would lie already at higher energy than the $\Sigma_u^-$ and $\Delta_u$ states in condensed phase, the avoided crossing would not take place. Hence, assigning the $^{3,1}\Pi_g$ transitions to the energy-loss features at 9.6 and 10 eV, the transitions from the ground state to the $\Delta_u$ valence states could be attributed to the features observed at about 8.5 eV. Although electronic transitions to $\Delta_u$ and $\Pi_g$ states are dipole forbidden in the linear geometry, they may still gain intensity or become allowed via vibronic coupling with the nearby $\Sigma_u^+$ and $\Pi_u$ states. In essence this mechanism stems from the fact that both $\Delta_u$ and $\Pi_g$ states, (i.e., one of the two degenerate components) correlate to $B_2$ states in the bent geometry with the lower energy one decreasing in energy with the bending angle while the upper one is increasing.[16, 18]

The energy-loss maximum at 8.9 eV observed in the 15-eV spectrum in Fig. 1(a) appears only as a shallow shoulder in the spectra at higher impact energies, as better seen in Fig. 1(b). Since at low incident energy the corresponding cross section is larger than that of the other structures already discussed, this strongly suggests that it could arise from an excitation to a triplet state. In the gas phase, Hall *et al.*[1] reported an energy-loss feature around 8.8 eV that was attributed to the $^3\Pi_g$ $(1\pi_g \rightarrow 3s\sigma_g)$ transition. In addition, McDiarmid and Doering observed at 8.9 eV an optically forbidden transition enhanced under electric quadrupole selection rules and suggested either a transition from the ground state to $A_2$ state in the bent molecule or the $\Pi_g$ state in the linear molecule.[3] However having already assigned the transitions to both $^{3,1}\Pi_g$ states to the feature around 9.8 eV, we propose for the feature at 8.9 eV the transitions to the $^{3,1}\Sigma_u^-$ valence states, which are predicted to have a singlet-triplet splitting smaller than 0.1 eV.[9, 12, 15-17] Besides, one may envisage a contribution from the transition to the $^1\Delta_u$ state, which is calculated to lie just above.[9, 12, 15-18] Although the $^{3,1}\Sigma_u^-$ transitions are dipole forbidden in both linear and bent geometry and strictly forbidden for electron scattering at both 0° and 180° (i.e., $\Sigma^+ \not\rightarrow \Sigma^-$ ),[28] they should be visible under the present scattering conditions of low-incident energy and large scattering angle. Considering that the $^{3,1}\Sigma_u^-$ states along with the $^1\Delta_u$ state are located at about 8.9 eV and given the singlet-triplet splitting of 0.4 – 0.6 eV for the $^{3,1}\Delta_u$ states, the $^3\Delta_u$ state should lie around 8.3 – 8.6 eV. However, in the electronic threshold spectrum of Cvejanovic *et al.*,[4] a vibronic stucture is superimposed on a continuous band around 8.4 eV. Because the vibrational spacing of 130 meV was not

characteristic of bending vibrations, but was similar to the stretching frequency in a Rydberg state, these authors tentatively assigned this band to the $^3\Pi_g$ Rydberg state. Assuming the same upward energy shift due to the condensed phase (i.e., 0.5 eV), we would expect this state to lie around 8.9 eV along with only the $^1\Pi_g$ state contributing to the energy loss around 9.8 eV. The main difficulty with this assignment is that it would imply a significantly larger $^{3,1}\Pi_g$ singlet-triplet splitting of 0.9 eV than what has been predicted by all of the calculations (i.e., 0.2 – 0.4 eV).[9, 12, 15, 16]

The $^3\Sigma_u^+$ valence state, which is generally believed to be the lowest in energy around 7.3 eV, has never been clearly observed in gas-phase electronic EEL spectra. No evidence for such a low-enegy transition is present in our results. But, considering that it could be located at a somewhat higher energy 8.04 – 8.35 eV, as suggested by the calculations of Nakatsuji[15] and Spielfiedel *et al.*,[16] the shallow shoulder around 7.9 eV, which can be more clearly seen in the difference spectrum Fig. 1(b), could be ascribed to this state.

Above 10.4 eV energy loss, the EEL spectra exhibit a sudden rise with an excitation energy threshold at 10.5 eV followed by a broad maximum around 10.8 eV, which is best seen in the 15-eV spectrum. In the gas phase spectra two sharp excitation bands are typically observed at 10.98 and 11.05 eV along with an energy threshold around 10.8 eV. Both bands have been assigned to the optically allowed transitions from the ground state to the $^1\Sigma_u^+$ ($\pi_g \rightarrow 3p\pi_u{}^*$) Rydberg-valence state. Judging from the present energy threshold value, the $^1\Sigma_u^+$ transition would be shifted to lower energy by about 0.3

eV in the condensed phase. Considering that such an energy shift could simply result from the electronic polarization of the surrounding medium combined with the large dipole strength of this transition, mostly suggest the presence of a valence character. In their optical absorption study of solid carbon dioxide, Abe and Onaka[8] reported a relatively sharp band at 10.68 eV. They ascribed this band to a molecular exciton related to a transition to the $^1\Sigma_u^+$ state that would be red-shifted by 0.31 eV in the solid phase. Similarly, Monahan and Walker reported a shift to lower energy by about 0.6 eV for this transition and explained it as being due to the local crystal field effects.[7]

The next feature, which is more visible in the 19.4-eV spectrum, appears as a shoulder around 11.75 eV. The latter corresponds to the second most intense feature observed at 11.38 eV in gas phase EEL spectra and that is assigned to an optically allowed transition to the $^1\Pi_u(\pi_u \rightarrow 3s\sigma_g{}^*)$ Rydberg state. Interestingly, the present upward energy shift of about 0.4 eV is just about the same as for the $^{3,1}\Pi_g$ $(1\pi_g \rightarrow 3s\sigma_g{}^*)$ transitions discussed above. In their optical absorption study of solid carbon dioxide, [7] Monahan and Walker had difficulty determining this transition, but assigned it to the faint feature around 11.2 eV. Still, Abe and Onaka reported,[8] besides the 10.68-eV peak above, other absorption bands at 11, 11.2, and 11.7 eV and that differ in numbers from those in the gas phase. This was explained essentially by the environment around a molecular site along with the intermolecular interaction in the crystal whose combined effect is to split the $^1\Sigma_u^+$ and $^1\Pi_u$ molecular electronic states into several energy levels in the crystal.[8]

Between 12.5 and 14.6 eV in the EEL spectra at $E_0$ = 19.4 and 25 eV, we observe a broad feature having its maximum around 13.4 eV. A similar feature has been reported

at about the same energy in the optical absorption spectrum of solid carbon dioxide by Abe and Onaka.[8] They proposed that it may arise from the higher members of a Rydberg series, which are found only around this energy in the gas phase. On the other hand, the first ionization potential of $CO_2$ is 13.776 eV in the gas phase.[25] Since this value should be lowered typically by about 1 eV in the condensed phase,[29] the same ionization process, but with its energy threshold at about 12.6 eV could well explain this feature. The decrease in intensity above 14.6 eV energy loss in the 19.4-eV spectrum, which differs from the 25-eV spectrum, results from the lower magnitude of the electronic excitation and ionization cross sections as they are probed closer to their energy threshold.

## IV. CONCLUSION

We have measured the electronic EEL spectra of solid film of $CO_2$ for incident electron energies of 15, 19.4 and 25 eV under small electron exposure and negligible sample damages. All sharp energy-loss peaks usually attributed to various Rydberg series in the gas phase has disappeared. In contrast, electronic transitions to the molecular valence $^{3,1}\Delta_u$ and $^{3,1}\Sigma_u^-$ states, which are dipole forbidden, remain practically the same in the solid phase. The valence $^1\Sigma_u^+$ transition, which is dipole allowed and exhibits large oscillator strengths, is shifted to lower energy by about 0.3 eV owing to the local crystal-field effects. On the other hand, transitions to mixed Rydberg-valence states, such as the $^{3,1}\Pi_g$ and $^1\Pi_u$ states, appear to be shifted to higher energy by about 0.4-0.5 eV in the solid phase in view of their Rydberg character in the linear geometry. Finally, the $^3\Sigma_u^+$ valence state, which is generally believed to be the lowest in energy around 7.3 eV in gas

phase, could lie at a somewhat higher energy around 7.9 eV as suggested by most of the calculations (Table I).

## ACKNOWLEDGMENTS

This work is supported by the Canadian Institutes of Health Research. We gratefully acknowledge the help provided by Mr. L. Parenteau and Dr. M. Lepage.

## REFERENCES

[1] R. I. Hall, A. Chutjian, and S. Trajmar, J. Phys. B **6**, L264 (1973).

[2] D. F. Dance, G. A. Keenan, and I. C. Walker, J. Chem. Soc. Faraday Trans. II **74**, 440 (1978).

[3] R. McDiarmid and J.P. Doering, J. Chem. Phys. **80**, 648 (1984).

[4] S. Cvejanovic, J. Jureta, and D. Cvejanovic, J. Phys. B **18**, 2541 (1985).

[5] M.-J. Hubin-Franskin, J. Delwiche, B. Leclerc, and D. Roy, J. Phys. B **21**, 3211 (1988).

[6] M. A. Green, P. J. O. Teubner, L. Campbell, M. J. Brunger, M. Hoshino, T. Ishikawa, M. Kitajima, H. Tanaka, Y. Itikawa, M. Kimura, and R. J. Buenker, J. Phys. B **35**, 567 (2002).

[7] K. M. Monahan and W. C. Walker, J. Chem. Phys. **61**, 3886 (1974).

[8] H. Abe and R. Onaka, J. Phys. Soc. Jpn. **53**, 1176 (1984).

[9] N. W. Winter, C. F. Bender, and W. A. Goddard III, Chem. Phys. Lett. **20**, 489 (1973).

[10] W. B. England, B. J. Rosenberg, P. J. Fortune, and A. C. Wahl, J. Chem. Phys. **65**, 684 (1976).

[11] W. B. England, W. C. Ermler, and A. C. Wahl, J. Chem. Phys. **66**, 2336 (1977).

[12] W. B. England and W. C. Ermler, J. Chem. Phys. **70**, 1711 (1979).

[13] W. B. England, Chem. Phys. Lett. **78**, 607 (1981).

[14] N. Padial, G. Csanak, B. V. McKoy, and P. W. Langhoff, Phys. Rev. A **23**, 218 (1981).

[15] H. Nakatsuji, Chem. Phys. **75**, 425 (1983).

[16] A. Spielfiedel, N. Feautrier, C. Cossart-Magos, G. Chambeau, P. Rosmus, H.-J. Werner, and P. Botschwina, J. Chem. Phys. **97**, 8382 (1992).

[17] C.-H. Lee, C. Winstead, and V. McKoy, J. Chem. Phys. **111**, 5056 (1999).

[18] R. J. Buenker, M. Honigmann, H.-P. Lieberman, and M. Kimura, J. Chem. Phys. **113**, 1046 (2000).

[19] L. Sanche and M. Michaud, Phys. Rev. B**30**, 6078 (l984).

[20] M. Michaud, P. Cloutier, and L. Sanche, Rev. Sci. Instrum. **66**, 2661 (1995).

[21] G. Bader, G. Perluzzo, L.G. Caron, and L. Sanche, Phys. Rev. B**26**, 6019 (1982).

[22] M. Falk and P. Seto, Can. J. Spectrosc. **31**, 134 (1986); M. Falk, J. Chem. Phys. **86**, 560 (1987).

[23] M. C. Deschamps, M. Michaud, and L. Sanche, (to be published).

[24] W. L. Jorgensen and L. Salem, *The Organic Chemist's book of orbitals* (Academic, New York, 1973).

[25] I. Reineck, C. Nohre, R Maripuu, P. Lodin, S. H. Al-Shamma, H Veenhuizen, L Karlsson, and K. Siegbahn, Chem. Phys. **78**, 311(1983).

[26] M.B. Robin, *Higher excited states of Polyatomic Molecules*, Vol. III, (Academic, New York, 1974).

[27] G. Herzberg, *Electronic Spectra of Polyatomic Molecules* (Van Nostrand, New Jersey, 1966).

[28] D. C. Cartwright, S. Trajmar, W. William, and D. L. Huestis, Phys. Rev. Lett. **27**, 704 (1971).

[29] M. Michaud and L. Sanche, J. Electron. Spectrosc. Relat. Phenom. **51**, 237 (1990).

II. 2. ARTICLE no 2 : Low-energy electron scattering cross section for the production of CO within solid films of carbon dioxide

# Low-energy electron scattering cross section for the production of CO within solid films of carbon dioxide

**M. C. Deschamps, M. Michaud and L. Sanche†**

Groupe des Instituts de Recherche en Santé du Canada en Sciences des Radiations, Université de Sherbrooke, Sherbrooke, Québec, Canada J1H 5N4

## Abstract

We report absolute electron scattering cross sections for the production of CO within thin solid film of carbon dioxide ($CO_2$) condensed on a solid Ar substrate. The CO fragments, which remain trapped within the bulk of the carbon dioxide film, are detected in situ by recording energy losses to their lowest triplet electronic state $a^3\Pi$ using high-resolution electron energy-loss spectroscopy. The production of CO is studied as a function of the electron exposure, film thickness and incident electron energy between 2 and 30 eV, a range within which most of the secondary electrons are created in systems irradiated by high energy particules. The energy dependence of CO production is characterized by a small feature around 4.5 eV with an absolute cross section $\sigma_p = (7.0 \pm 4.0) \times 10^{-18}$ cm$^2$, a minimum around 7 eV, a strong rise from 8 eV up to a maximum $\sigma_p = (5.4 \pm 2.5) \times 10^{-17}$ cm$^2$ at 15 eV, a decrease with a minimum around 19, and finally a slowly and monotonically increase above 20 eV. The CO production is discussed in terms of the formation of electron resonances, which may lead directly to the fragmentation of the molecule via dissociative electron attachment or indirectly by decaying into an entirely repulsive part of corresponding excited neutral and positive ion states.

KEYWORDS: carbon dioxide, electron, condensed phase, dissociation, cross section

†Canada Research Chair in the Radiation Sciences

## I. INTRODUCTION

The carbon dioxide molecule ($CO_2$) is one of the most studied polyatomic molecules. It has been investigated by almost all the spectroscopic techniques available. Its relevance is found in a wide range of circumstances. These include the implication of $CO_2$ chemistry in atmospheres of Mars, Venus and Earth, the interstellar medium,[1, 2] and the environment as well as in global warming processes, laser discharges,[3] plasmas, radiation damage and radioprotection.[4] Furthermore, because its simplicity, $CO_2$ presents a theoretical interest for the development of modeling and calculations in molecular physics.

The study of collisions of low-energy electrons with the $CO_2$ molecule is essential to develop a better understanding of the energy transfer to molecules, more particularly those leading to bond breakage or fragmentation. Electron-molecule scattering is conveniently divided into resonant and non-resonant (*i.e.*, direct) processes. A resonant process or the formation of a transient anion is initiated by the temporary capture of an electron into a previously unfilled orbital of an atomic or molecular target in its ground or excited states. Thus, in such a process, the electron resides on the target for a time much longer than the usual direct scattering time. A transient anion state may decay via either (a) electron autodetachment with the target in the ground or an excited electronic state, (b) dissociation into an anion and one or more neutral fragments, or (c) by stabilization of the anion. Vibrational and electronic excitation as well as dissociation cross sections are considerably affected by the presence of resonances as opposed to non-resonant (*i.e.*, direct) cross sections, which generally show a smooth and a slowly varying energy dependence.[5]

Formation and decay of electron resonances in $CO_2$ have been extensively studied in the gas and cluster phases. More recently, the study of these resonance processes was also carried out for condensed $CO_2$. Studies of the condensed or physisorbed phase are important to understand how the decay channels along with their branching ratios can be altered by the molecular environment. More particularly in our laboratory, we have investigated some $e^- + CO_2$ reaction pathways in the condensed phase by means of charge trapping experiments using low-energy electron transmission (LEET) spectroscopy[6] and electron stimulated desorption (ESD) measurements of $O^-$ and metastable CO*.[7] More recently, we investigated by electron energy loss (EEL) spectroscopy the electronic states of $CO_2$ in the condensed phase.[8]

In the present paper, we report on the production of neutral CO fragments resulting from low-energy electron bombardment on thin films of $CO_2$ condensed at 18 K on a solid argon substrate. As in previous works,[9, 10] EEL spectroscopy is used to detect and identify *in situ* the neutral fragmentation products. The production of CO, which is clearly identified via its lowest triplet electronic state $d^3\Pi$, is studied as a function of the electron dose, incident electron energy, and thickness of the deposited film. The energy dependence of the CO production rate between 2 to 30 eV is also calibrated in terms of an electron scattering cross section. The structures in the CO signal are related to the formation of several electron resonances. If sufficiently long lived and at least partially repulsive, these transient anion states may induce dissociation of the molecule into a stable negative ion along with one or more neutral fragments [*i.e.,* dissociative electron attachment (DEA)]. Otherwise, if resonance decay is dominated by electron autodetachment, fragmentation into neutral species may still occur. Such fragmentation

requires the molecule to be left into an entirely repulsive part of the potential energy surface of the corresponding excited neutral or positive ion states, lying above the dissociation limit of the fragments.

## II. EXPERIMENT

The experiments were performed with a high-resolution electron-energy-loss spectrometer consisting of two hemispherical electrostatic deflectors (*i.e.*, monochromator and analyzer) as previously described in detail.[11] The angle of incidence $\theta_0$ can be varied between 8° and 80° from the normal to the sample. The angle of analysis $\theta_d$ is fixed at 45° at the opposite azimuth. Double-zoom electrostatic lenses at the exit of the monochromator and at the entrance of the analyzer allow constant focusing and beam size over a wide incident energy range (*e.g.*, 2 – 30 eV) along with minimum variations of the instrument transmission. The apparatus is housed in a μ-metal UHV chamber maintained at a base pressure of 1 x $10^{-10}$ Torr by an ion pump and a liquid-$N_2$ cooled titanium sublimation pump. In the present experiment, the combined resolution of the selectors was set at 15 meV full width at half maximum (FWHM) for a current $I_0$ = 0.12 nA incident on the substrate. This incident current, which is monitored with an electrometer connected to the substrate, is calibrated by comparison to the current measured through a sample of known transmission. The incident electron energy $E_0$ was calibrated within ±0.1 eV with respect to the vacuum level by measuring the threshold of the electron current transmitted through the samples.

The samples are initially prepared in a gas-handling manifold that consists of three gas or vapor sources connected through bypass and precision-leak valves to a small

calibrated volume. The absolute pressure in this volume is measured with a capacitance manometer. For each deposited sample, a known amount of gas or vapor, which is measured by the differential pressure drop in the calibrated volume, is leaked via a stainless steel capillary whose end is located just in front of a Pt(111) single crystal. The crystal is mounted on a sample manipulator,[12] which allows azimuthal rotation, flip and X, Y and Z translations of the sample. The crystal is held at a temperature of 18 K via a flexible copper braid attached to the cold head of a close-cycle helium refrigerator (APD Cryogenics Inc. Allentown, PA). Crystal cleaning is achieved by resistive heating at 1100 K and sequences of $Ar^+$ sputtering followed by annealing and heating in the presence of oxygen at about 900 K.

Carbon dioxide and carbon monoxide gases were supplied by Matheson of Canada Ltd. with a stated purity of 99.9995 % and 99.99%, respectively. The number of condensed layers of $CO_2$ was estimated within 20% from the calibrated amount of gas needed to deposit a monolayer, assuming the same sticking coefficient and growth mode for the adlayers, as described previously.[13] Carbon dioxide gas is known to condense between 10 and 30 K as a metastable amorphous solid film that transforms irreversibly to the crystalline form upon annealing to 50 – 77 K.[14] The absence of a strong electron elastic reflectivity in the specular direction (*i.e.,* the elastic reflectivity at $\theta_0 = 45^\circ$ being similar to that at $\theta_0 = 8^\circ$ ) indicated that our films consisted primarily of randomly oriented crystallites and/or amorphous material.

To prevent a possible decomposition of $CO_2$ on the Pt surface, as well as to rule out any insidious effect due to the proximity of the metal surface, a five-layer film of argon with a stated purity of 99.9995% (Matheson of Canada Ltd.) was systematically

used as a spacer. Film charging, which can be readily detected from slight changes in the threshold of the electron current transmitted through the film, was tolerated as long as it yielded a shift no larger than ± 0.1 eV on the incident electron energy scale.

## III. PRODUCTS FORMATION MODEL

In the simplest case, the formation of products induced by low-energy electrons within a sample is described by a single-event process. That is, an electron transfers its energy or part of it to a molecule, which then dissociates or fragments without further reaction with neighboring molecules. Let us consider an electron beam $I_0$ characterized by an uniform current density $i_0 = I_0 / S_0$ within an area $S_0$ and $i_0 = 0$ outside being incident on a film of molecular number density $n_0$ and thickness $L$. Assuming a negligible electron beam attenuation into the film, the amount of fragments arising from electron exposure for a sufficiently small time $t$, is given by

$$p_t S_0 L = n_0 \sigma_p L I_0 \times t \quad . \tag{1}$$

In this relation, $p_t$ is the concentration of fragments in the film after a time $t$ and $\sigma_p$ is the cross section for the formation of a specific fragment induced by electron at a given impact energy. Thus the amount of fragments formed within the area $S_0$ and over the thickness $L$ per unit time (*i.e.,* the production rate) corresponds to the combined factors, $n_0 \sigma_p L I_0$, in front of the independent variable $t$.

The appearance of fragments in a film can be probed *in situ* with the same incident electron beam by measuring the scattered electron current $J^*$ arising from a vibrational or electronic excitation (*i.e.*, signal intensity) that is specific to the fragment. Considering again negligible electron beam attenuation and an electron-fragment scattering cross

section $\sigma^*$, the signal $J^*$arising from the fragments is simply given by

$$J^* = p_t \sigma^* L I_0 = \left( \frac{\sigma^* I_0}{S_0} \right) n_0 \sigma_p L I_0 \times t \,, \tag{2}$$

upon using Eq. (1) resolved for $p_t$ in the right-hand side. Hence for sufficiently small electron exposures, $J^*$is a linear function of time and leads, within the constant factor in parentheses, to the production rate (*i.e.*, $n_0 \sigma_p L I_0$). Besides, $J^*$is directly proportional to the film coverage $n_0 L$. One must bear in mind, though, that the later behavior stems essentially from the neglect of the electron beam attenuation and more generally one should expect to see a departure from it at sufficiently high coverage.

## IV. RESULTS

### A. Energy-loss spectra and identification of CO

We have recently reported the electronic EEL spectra of solid film of $CO_2$ for incident electron energies of 15, 19.4 and 25 eV under small electron exposure and negligible sample damage.[8] All sharp energy-loss peaks usually attributed to various Rydberg series in the gas phase disappear whereas electronic transitions to the molecular valence $^{3,1}\Delta_u$ and $^{3,1}\Sigma_u^-$ states, which are electric dipole forbidden, remain practically the same in the solid phase. The valence $^1\Sigma_u^+$ transition, which is electric dipole allowed and exhibits large oscillator strengths, is shifted to lower energy by about 0.3 eV owing to the local crystal-field effects. On the other hand, transitions to mixed Rydberg-valence states, such as the $^{3,1}\Pi_g$ and $^1\Pi_u$ states, appear to be shifted to higher energy by about 0.4-0.5 eV in the solid phase in view of their Rydberg character in the linear geometry. Finally, the

$^3\Sigma_u^+$ valence state, which is generally believed to be the lowest in energy around 7.3 eV in gas phase, was ascribed to the lowest energy-loss feature in the solid at 7.9 eV.

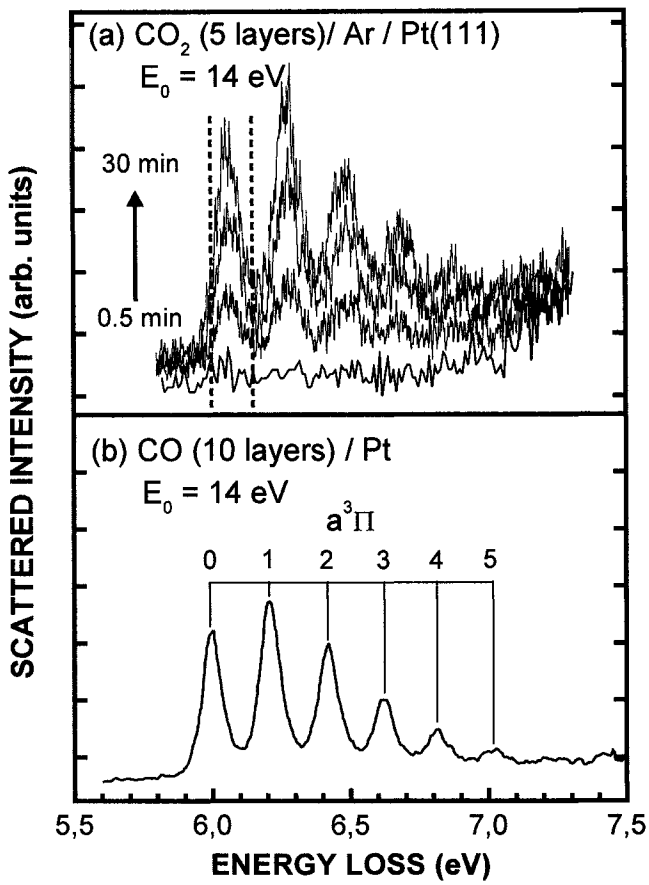


Fig. 1. Electron-energy-loss spectra recorded with 14 eV electrons incident on (a) a five-layer film of $CO_2$ condensed on a five-layer spacer of Ar. The film was exposed to electrons during 0.5 min for the lowest curve and 30 min for the highest curve. (b) a 10-layer film of CO condensed on a platinum substrate. The vibronic progression in condensed CO, which has a spacing of about 0.21 eV, corresponds to that found in the lowest electronic state $a^3\Pi$ of CO in the gas phase.

Fig. 1(a) shows the EEL spectrum from 5.8 to 7.1 eV of a five-layer film of $CO_2$ condensed on the five-layer spacer of argon. The film was exposed to 14-eV electrons during 0.5 min for the lowest curve and up to 30 min for the highest curve. Of particular

interest here is the vibronic progression appearing with the exposure, and which, except for being shifted by about 60 meV toward higher energy, corresponds to that found in the lowest electronic state $a^3\Pi$ of a 10-layer film of CO condensed on Pt as shown in Fig. 1(b).[15] The same shift was observed for mixture films composed of one to six percents of CO in $CO_2$. The present blue shift can be seen as an energy increase between the ground state and the $a^3\Pi$ valence electronic state of the CO molecule upon relocation into solid $CO_2$. Since solid $CO_2$ has an electronic polarizability comparable to that of solid CO, the valence electronic state is expected to be shifted slightly to lower energy by about the same amount in both case. In counterpart, the cohesive energy per molecule in solid $CO_2$ being larger than that in solid CO, implies that the molecular ground state should be found at somewhat lower energy in the former than in the later case, thus resulting in a larger transition energy in solid $CO_2$.

**B. Dependence of CO production on electron exposure and film thickness**

In principle, the appearance of the CO signal may be caused by dissociation of $CO_2$ induced by electron impact or by an external spurious sources, such as incandescent filaments, which may produce minute quantities of CO that may condensed on the sample surface. In the former case, the signal should vary with the electron exposure, electron energy, and film thickness, whereas in the latter case it should grow merely with time due to molecular adsorption on a film held at cryogenic temperature ($T < 23$ K). The amount of CO produced by 14 eV electrons incident on a five-layer film of $CO_2$ deposited on the Ar spacer is shown as a function of the electron exposure or bombardment time in Fig. 2. The data were obtained from the $v = 0$ of the $a^3\Pi$ state of CO integrated between 6.00 and 6.15 eV in the $E_0 = 14$ eV EEL spectrum [vertical dashed lines in Fig. 1(a)]. Each of

these points actually results from only 0.5 min recording time in order to minimize the effect of the electron beam during probing of the damage. The break in the horizontal axis represents a delay of 15 min, during which the electron beam was turned off, but all the filaments in the vacuum system remained incandescent. The observed continuity in the data rules out the possibility that the CO signal could arise from spurious sources nor that CO could sublimate significantly from our films during the course of an experiment.

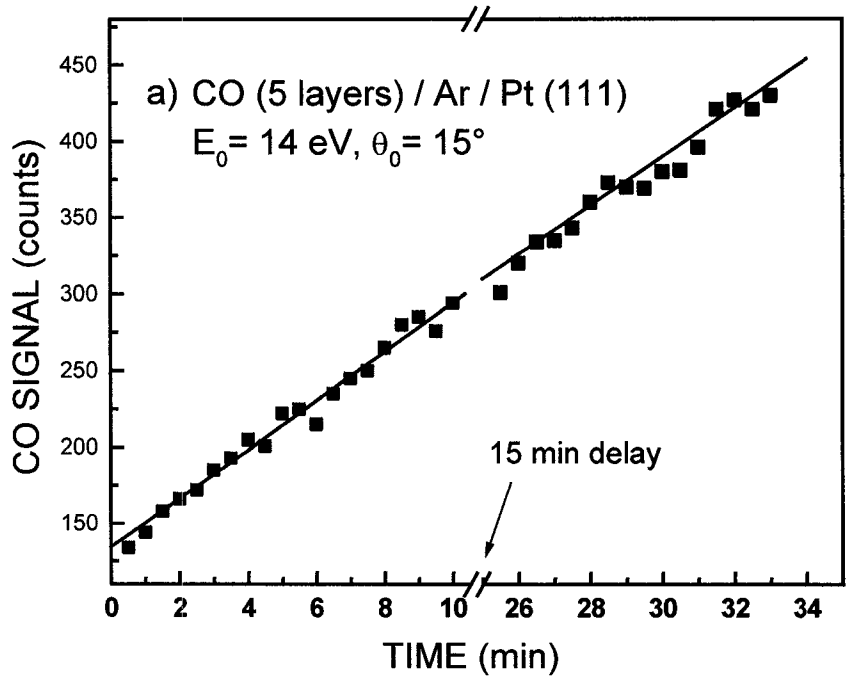


Fig. 2. Evolution of the CO signal integrated between 6.00 and 6.15 eV [vertical dashed lines in Fig. 1(a)] produced by 14 eV electrons incident on the five-layer film of $CO_2$ deposited on the Ar spacer. The continuity in the CO signal after a 15 min delay in which the electron beam was off but all the filaments remain incandescent rules out the possibility that CO could come from spurious sources nor that CO could sublimate significantly during the course of an experiment.

The same CO signal (*i.e.,* integrated v = 0 intensity in the $E_0$ = 14 eV EEL spectrum) as a function of bombardment time is shown for three different incident energies $E_0$ = 10, 14 and 24 eV in Fig. 3. For all energies the CO signal increases linearly during the first 35 min of bombardment. The departure from the linear behavior, which occurs typically after 40 min at 14 eV, is mainly attributed to film charging. The slope of the straight line passing through each data set gives, within a constant factor [c.f., Eq. (2)], the CO production rate at the bombarding energy.

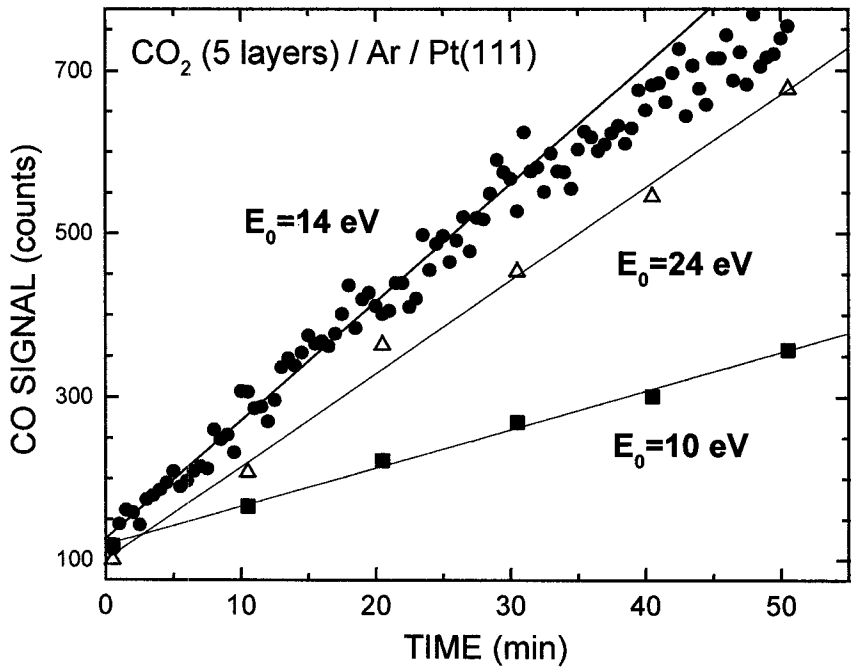


Fig. 3. Evolution of the CO signal for electron incident on a five-layer film of $CO_2$ deposited on a five-layer Ar spacer for three different incident energies. The CO signal corresponds to the signal integration between 6.00 and 6.15eV of energy loss measured with an incident electron energy of 14 eV over 0.5 min. The solid lines represent a linear fit to the data and correspond, within a constant factor, to the CO production rate for each incident energy.

We show in Fig. 4 the CO production rate at a fixed incident energy of 14 eV (*i.e.,* the slope values in Figs. 2 and 3) as a function of the film thickness of $CO_2$ condensed on

the Ar spacer. The error bars indicate the standard deviation of the linear fit to the experimental data and do not include the systematic uncertainty in the number of deposited layers (*i.e.,* 20%). The rise in the production rate with increasing film thickness indicates that CO is found in the bulk and not only at the surface of the film. Furthermore, the observed linear behavior up to about 6 layers strongly suggests negligible electron beam attenuation within the film along with a fragmentation process that stems initially from individual molecular sites (*i.e.,* single event). Above 6 layers attenuation of the electron beam is no longer negligible and corresponds to a depth beyond which the newly formed molecules in a film cannot be probed or detected efficiently. For electrons that enter, scatter once on specific molecules, and then leave the film, thus generating a backscattered signal, this *probed depth* corresponds to half of the average of the electron mean free paths at the initial and final electron energies.

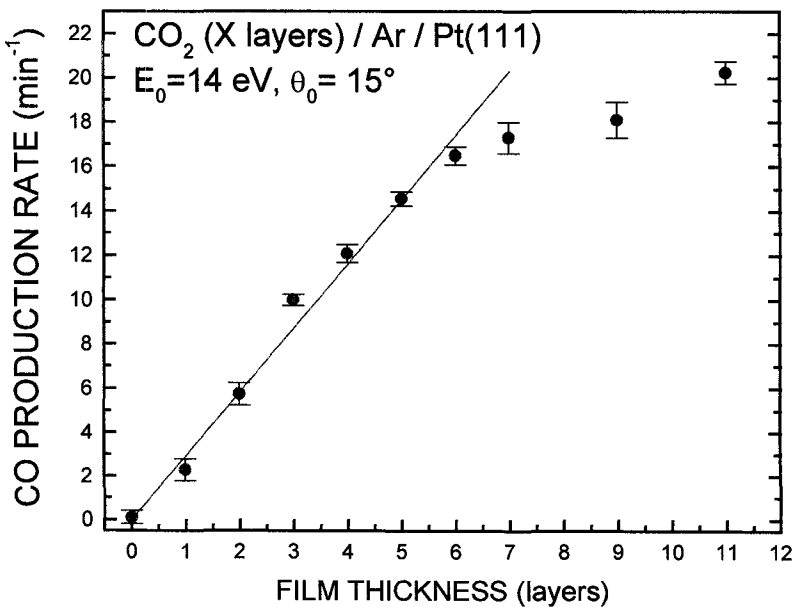


Fig. 4. The rate of CO production in films of condensed $CO_2$ on an Ar spacer as measured by the slope in Fig. 3 but for different film thickness.

To quantify the amount of CO produced within a film, the CO signal (*i.e.*, integrated v =1 intensity in the $E_0$ = 14 eV EEL spectrum) was compared to that obtained from probing several films of $CO_2$ containing up to 6% of CO (*i.e.*, mixture films). These mixture films were deposited on the Ar spacer with the same thickness $L$ as for the exposure experiments. Taking the incident electron current $I_0$ on a mixture film and the electron-CO scattering cross section $\sigma^*$ as being the same as those in an exposure experiment, the scattered current $J^*$ arising from CO in the mixture reads

$$J^* = n_{CO}\sigma^* L I_0 = n_0\sigma^* L I_0\left(\frac{n_{CO}}{n_0}\right). \quad (3)$$

In this expression $n_{CO}$ is the concentration of CO in a mixture film of number density $n_0$. Thus for a given film thickness, the intensity of the CO signal (*i.e.*, $J^*$) is predicted to follow a linear relationship with the normalized concentration of CO (*i.e.*, $n_{CO}/n_0$) in %. This is also observed experimentally as shown in Fig. 5. Besides, the slope of the straight line passing through the experimental data corresponds to the value of the combined factor, $n_0\sigma^* L I_0$, in Eq. (3). Dividing Eq. (2) by this factor, the intensity $J^*$ of the CO signal in counts, as obtained from an electron exposure experiment, can be readily converted into a normalized concentration of CO produced in the film (*i.e.*, $p_t/n_0$) in %, as

$$\frac{J^*}{n_0\sigma^* L I_0} = \frac{p_t}{n_0} = \frac{\sigma_p I_0 t}{S_0}. \quad (4)$$

In contrast to $J^*$, which reflects the *amount* of CO within a film, we note that $p_t/n_0$ does not depend explicitly on the film thickness and is also directly proportional to the cross section.

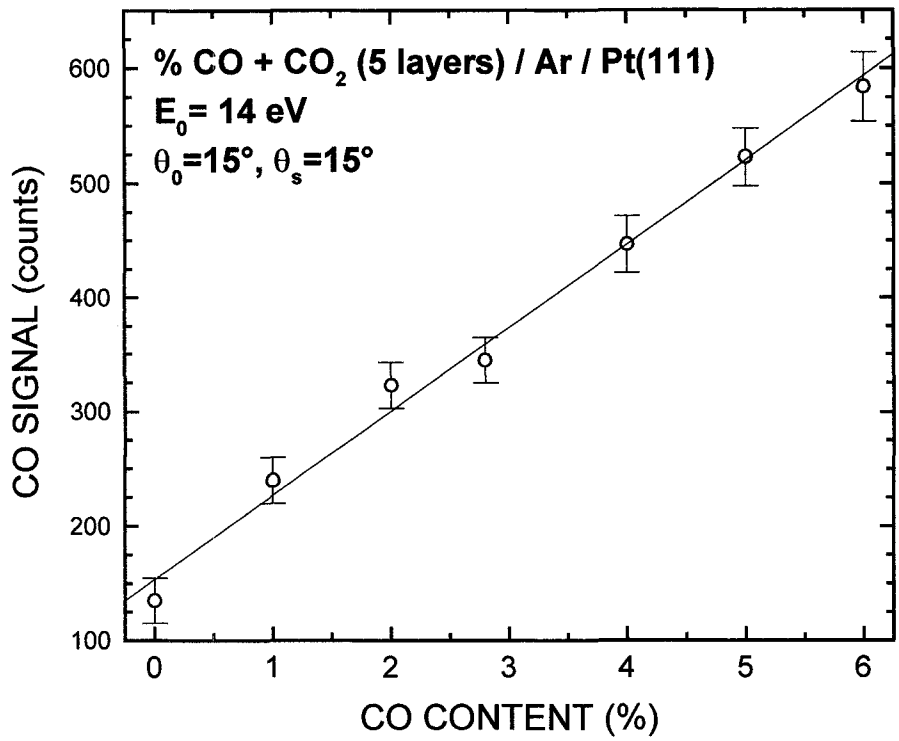


Fig. 5. CO signal integrated over the same spectral range and recorded on 5-layer films of reference mixtures containing various amount of CO.

### C. Dependence on incident electron energy

Given the correspondence between the intensity of the CO signal and the normalized concentration of CO (Fig. 5) in a mixture film, we show in Fig. 6 the normalized production rate of CO in a five-layer film of $CO_2$ deposited on the Ar spacer (*i.e.*, $p_t/n_0 t$ in % per min) as a function of the incident electron energy. Each energy point derives from the slope of a straight line passing through the experimental data probed at 14 eV, as shown in Fig. 3. The energy dependence is characterized by a small feature around 4.5 eV, a minimum around 7 eV, a strong rise from 8 eV up to a maximum at 15 eV, a decrease with a minimum around 19, and finally a slowly and monotonically increase

above 20 eV. For each energy, electron bombardment and signal probing were performed on a new film deposition, which may admit 10% variation in the thickness, and the zoom lenses of the spectrometer were optimized to ensure a constant incident current and beam size at the sample. It should be noticed that the observed minimum rate is due to fragmentation accumulated during the probing time at $E_0$ = 14 eV and thus is intrinsic to the measurement. As such it should correspond to a fraction of the value obtained at 14 eV. Following from the present bombardment and probing times with the ratio 0.5 min /(10 + 0.5) min, this fractional part is represented by an horizontal dashed line in Fig. 6 and sets the zero of the cross section scale.

**D. Cross section calibration**

The absolute cross section for the production of CO can be readily obtained from the normalized CO production rate (*i.e.*, $p_t/n_0 t$) determined above, upon solving Eq. (4) for $\sigma_p$ as

$$\sigma_p = \left(\frac{p_t}{n_0 t}\right)\frac{S_0}{I_0}. \qquad (5)$$

where $I_0$ is the incident electron beam current and $S_0$ the area irradiated by the electron beam at the surface of the film.[9, 10]

To determined $S_0$, three films of $CO_2$ were bombarded during 30 minutes at different impact energies of $E_0$ = 10, 14 and 19 eV, respectively. After each bombardment, the same CO signal (*i.e.*, integrated v = 0 intensity in the $E_0$ = 14 eV EEL spectrum) was measured as a function of the $X$ and $Y$ position of the sample. The three resulting intensity profiles are presented relative to their respective maximum in Fig. 7. All profiles are

characterized by a triangular shape with a FWHM of 0.6 ± 0.04 mm and 0.2 ± 0.02 mm in the $X$ and $Y$ directions. These results insure that both the position and the size of the irradiated area at the sample were kept reasonably constant between $E_0$ = 10 and 19 eV. They further indicate that the amount of CO produced is practically constant over the rectangular area delimited by the electrostatic image of the rectangular exit slit of the monochromator at the sample. From these results, the irradiated area is evaluated to be $S_0$ = 1.2 x $10^{-3}$ $cm^2$ ± 0.2 x $10^{-3}$ $cm^2$.

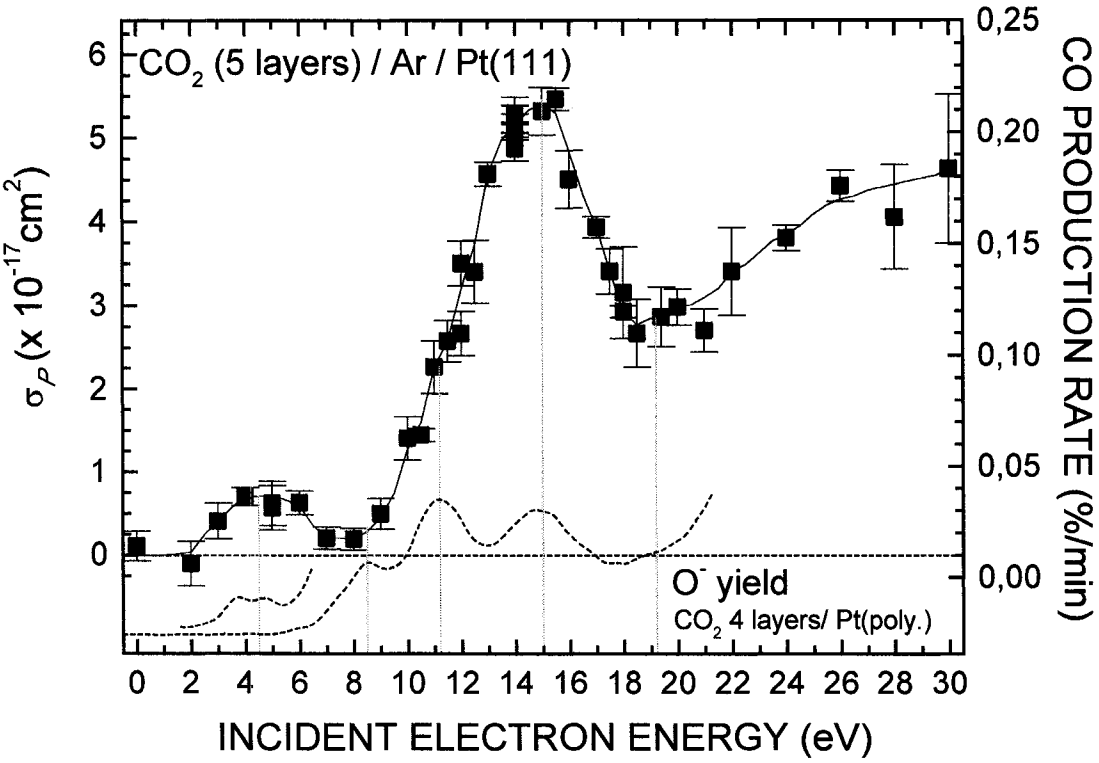


Fig. 6. CO production rate in five-layer films of condensed $CO_2$ on an Ar spacer as function of the electron incident energy. The left vertical scale gives the absolute cross section $\sigma_p$ for the production of CO. The shape of the $O^-$ yield spectra of a four-layer film of $CO_2$ measured by Huels *et al.* is reproduced at the bottom of the figure for comparison. The structure around 4 eV in the $O^-$ yield only appeared when the film was allowed to charge negatively.

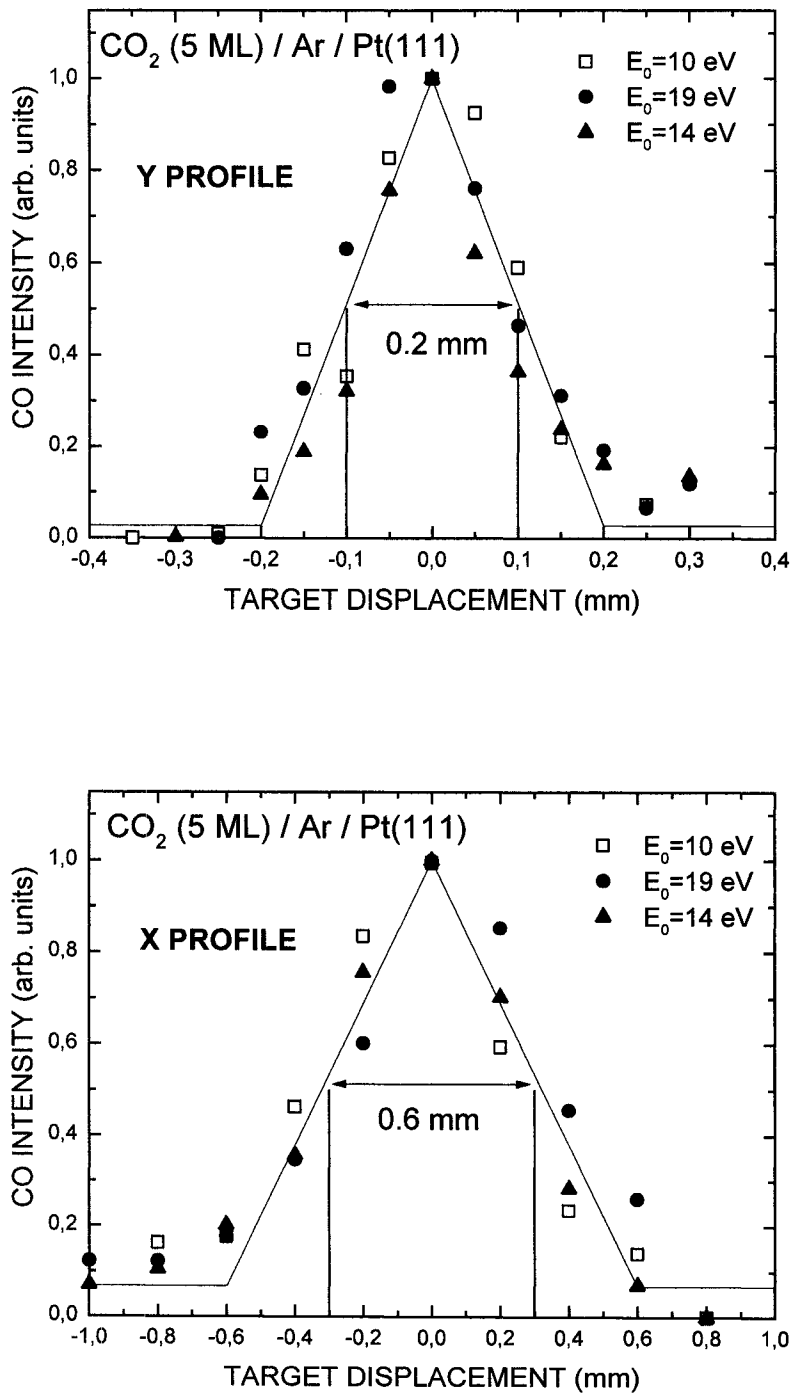


Fig. 7. Intensity of integral CO signal measured at 14 eV along the X and Y directions after 30 minutes of electron impact at $E_0$ = 10, 14 and 19 eV. The triangular shaped profiles indicate a nearly constant electron density over a rectangular area of 6 mm by 2 mm.

Small shift and distortion in the $X$ and $Y$ profiles were found around 4 eV and consequently the production rate at low energies (2-6 eV) is slightly underestimated. This distortion could be explained by a film charging resulting from the dissociation. Indeed, the fragmentation of $CO_2$ via DEA leads to the production of $O^-$. Though, because of the small kinetic energy ($E_k$) available to $O^-$ at 4 eV,[16] $O^-$ initially gets trapped in the film and charges it.[7]

Given the value of the irradiated area and the incident current at the surface $I_0 = (0.12 \pm 0.03)$ nA, the normalized production rate is readily converted to an absolute cross section value ($cm^2$) for each incident energy by referring on the left-vertical scale in Fig. 6. For $E_0 = 14$ eV, we find a cross section $\sigma_p = (5.3 \pm 2.5) \times 10^{-17}$ $cm^2$.

## V. DISCUSSION

Early studies of dissociative attachment in $CO_2$ gas revealed two intense $O^-$ bands around 4.4 eV and 8.2 eV [17, 18] having cross sections at their respective maxima of $1.4 \times 10^{-19}$ $cm^2$ and $4.5 \times 10^{-19}$ $cm^2$ followed by three weak peaks around 13 eV, 17 eV and 19.4 eV all having cross sections of about $1 \times 10^{-20}$ $cm^2$.[16, 19] ESD of $O^-$ and metastable CO* from physisorbed $CO_2$ found evidences for at least five resonances below 20 eV at incident energy of 4.1, 8.5, 11.2, 15 and 19.2 eV.[7] According to the works of Stamatovic and Schulz,[20] and Abouaf *et al.*,[21] the cross section of the $O^-$ yield in the gas phase around 4 eV exhibits vibrational structure. Stamatovic and Schulz attributed the structure to the formation of vibrationally excited CO fragments. Abouaf *et al.* pointed out that the spacing do not correspond to the vibrational levels of the CO and suggested that the observed structure may be connected to the capture rather than with the decay. A more recent paper showed that both mechanisms contribute to the observed structures.[22]

In the present experiment, we observe a maximum between 3 and 6 eV with a cross section of $\sigma_p = (7.0 \pm 4.0) \times 10^{-18}$ cm$^2$. This structure can be associated as in the gas phase with a short lived $^2\Pi_u$ shape resonance in $CO_2$ which dissociates into $O^-(^2P)$ and $CO(X^1\Sigma^+)$ fragments.[23]

$$CO_2(X\,^1\Sigma_g^+) + e \rightarrow CO_2^-(^2\Pi_u) \rightarrow CO(X\,^1\Sigma^+) + O^-(^2P) \quad (6a)$$

Onset for this process was found in the gas phase to be around 3.97 eV.[20, 21, 24] In condensed phase, the threshold is shifted to lower energy as observed in the present experiment and by the $O^-$ yield measured by Huels *et al.*[7] This shift is expected owing to the effect of the electronic polarization on both the $CO_2^-$ $^2\Pi_u$ transient anion state and the anion fragment $O^-$.

Instead of a $^2\Pi_u$ shape resonance, Cartwright and Trajmar have recently suggested that a Feshbach core-excited resonance with a bent nuclear geometry could also explain DEA in the 3.5-5.0 eV energy region.[25]

The DEA to $CO_2$ in gas phase is known to be dominated by a strong maximum at 8.2 eV. This process was associated in early works to $^2\Sigma^+$ shape resonance[23] of $CO_2^-$, but more recent works[7, 19, 22] suggest a $^2\Pi_g$ mixed valence-Rydberg state with a $^{1,3}\Pi_g$ parent state.

$$CO_2(X\,^1\Sigma_g^+) + e \rightarrow CO_2^-{}^*(^2\Pi_g) \rightarrow CO(X\,^1\Sigma^+) + O^-(^2P) \quad (6b)$$

The $^{1,3}\Pi_g$ parent states of $CO_2$ were found to be blue shifted by 0.5 eV in the condensed phase.[8] This shift is reflected in the position of the resonance in the condensed phase as observed via the $O^-$ yield,[7] where the maximum appeared around 8.5 eV. The $O^-$ yield also showed that this resonance is no longer the dominating structure in the condensed phase.

The energy scale step in the actual CO production rate does not allow us to resolve a structure for this resonance. The intensity of this structure is probably too weak compared to the following one and to close to it. Moreover, it was found that the fragments of this DEA process were formed with considerable kinetic energy at onset.[16, 23, 26] Indeed, the CO fragments produced have sufficient energy to diffuse out of the film and thus lower the measured CO signal.

As mentioned above, the $O^-$ yield in condensed phase is no longer dominated by the 8 eV resonance as in the gas phase. Instead, the two maxima at 11.2 eV and 15 eV are the most intense structures.[7] In the cross section for the production of CO, we find a very intense feature arround 15 eV with a maximum value of $\sigma_p = (5.4 \pm 2.5) \times 10^{-17}$ cm$^2$. Its large width in energy suggests the presence of more than one resonance leading to the following DEA processes:[26]

$$CO_2(X\,^1\Sigma_g^+) + e \rightarrow CO_2^-{}^* \rightarrow CO(X\,^1\Sigma^+) + O^-(^2P) \qquad (6c)$$

$$CO_2(X\,^1\Sigma_g^+) + e \rightarrow CO_2^-{}^* \rightarrow CO^*(a\,^3\Pi) + O^-(^2P)\ . \qquad (6d)$$

In addition to DEA processes, neutral CO fragments could also be produced by neutral dissociation resulting from the excitation of $CO_2$ into repulsive part of an excited state. Such an excitation could occur via direct excitation or resonance scattering (*i.e.*, the decay of a $CO_2^-$ state into an excited state of $CO_2$ which is dissociative). For example, it is known that the $CO_2$ ($^1\Sigma_u^+$) state dissociates to O($^1$S) and CO ($X\,^1\Sigma^+$),[27, 28]

$$CO_2(X\,^1\Sigma_g^+) + e \rightarrow CO_2^*(^1\Sigma_u^+) + e \rightarrow CO(A\,^1\Sigma^+) + O(^1S) + e\ . \qquad (6e)$$

LeClair and McConkey[28] measured the cross section for the production of $O(^1S)$ originating mainly from reaction (6e). They found a threshold energy of 11 eV corresponding to the excitation energy of the $CO_2$ $(^1\Sigma_u^+)$[29] along with a smoothly increasing cross section up to about 60 eV. LeClair and McConkey[28] listed several other neutral dissociations having a dissociation limit below 16 eV and thus susceptible to contribute to the CO production rate.

The lowest energetic dissociative ionization of $CO_2$ involved the formation of CO and $O^+$ as[30]

$$CO_2\,(X\,^1\Sigma_g^+) + e \rightarrow CO + O^+ + 2e \quad . \tag{6f}$$

The thermodynamic onset for this reaction is calculated at 19.069 eV.[31] Several electroionization and photoionization mass spectrometry experiments in the gas phase confirm this value.[32-37] This energy threshold is expected to be lowered by about 1 eV in the condensed phase owing to the electronic polarization around the positive ion. Thus, the CO production rate above 18eV should contains contribution of dissociative ionization.

## VI. CONCLUSION

Fragmentation in solid $CO_2$ film condensed at 18 K on a Pt surface previously cover with Ar was induced and monitored using a high resolution low electron energy loss spectrometer. Neutral CO fragments which remain in the bulk of the film were monitored via the $a^3\Pi$ excited state of CO using the same apparatus. CO production rate was deduced by comparing the intensity of CO produced with the CO intensity of films of

reference mixtures containing up to 6% of CO. The production rate was then calibrated in term of an absolute cross section. The production rate of CO was found to increase linearly with the number of condensed layers of $CO_2$. It indicates a single-event process and that the magnitude of the CO yield is similar at the surface and within the bulk of $CO_2$ films. Thus, caging effects, which often considerably reduce reaction rates within condensed matter do not seem to have appreciable consequences on dissociative processes within solid $CO_2$.

The CO production rate was studied as a function of the incident electron energy over 2-30 eV range. It was characterized by a maximum around 4 eV which was assigned to the $^2\Pi_u$ resonance state of $CO_2^-$ previously observed in the gas phase. The threshold in the condensed phase, however, was found to be lower than in the gas phase. More over, the cross section measured for this resonance $\sigma_p = (7.0 \pm 4.0) \times 10^{-18}$ cm$^2$ is about 50 times higher in the solid phase than in the gas phase. Whereas in the gas phase the dissociative electron attachment resonance around 8.2 eV dominates the CO production, in the condensed phase the latter is dominated by a strong maximum at 15 eV with a cross section of $\sigma_p = (5.4 \pm 2.5) \times 10^{-17}$ cm$^2$.

## ACKNOWLEDGMENTS

This work is supported by the Canadian Institutes of Health Research. We gratefully acknowledge the help provided by Mr. L. Parenteau and Dr. M. Lepage.

## REFERENCES

[1] S.K. Bhattacharya, J. Savario, and M.H. Thiemens, Geophysical Research Letters **27**, 1459 (2000).

[2] L.G. Christophorou, *Electron-Molecule Interactions and their Applications* (Academic, New York, 1984), Vol. 1, Chap. 1 and 2.

[3] L.G. Christophorou and S.R. Hunter, *Electron-Molecule Interactions and their Applications* (Academic, New York, 1984), Vol. 2, p 320.

[4] M. Spotheim-Maurizot, J. Franchet, R. Sabattier, and M. Charlier, Int. J. Radiat. Biol. **59**, 1313 (1991).

[5] L. Sanche, J. Phys. B **23**, 1597 (1990).

[6] M. A. Huels, A. D. Bass, P. Ayotte, and L. Sanche, Chem. Phys. Letters **245**, 387 (1995).

[7] M. A. Huels, L. Parenteau, P. Cloutier, and L. Sanche, J. Chem. Phys. **103**, 6775 (1995).

[8] M. C. Deschamps, M. Michaud, and L. Sanche, to be published.

[9] M. Lepage, M. Michaud, and L. Sanche, J.Chem.Phys. **113**, 3602 (2000).

[10] M. Lepage, M. Michaud, L. Sanche, J.Chem.Phys. **107**, 3478 (1997).

[11] L. Sanche and M. Michaud, Phys. Rev. B**30**, 6078 (1984).

[12] M. Michaud, P. Cloutier, and L. Sanche, Rev. Sci. Instrum. **66**, 2661 (1995).

[13] G. Bader, G. Perluzzo, L.G. Caron, and L. Sanche, Phys. Rev. B**26**, 6019 (1982).

[14] M. Falk and P. Seto, Can. J. Spectrosc. **31**, 134 (1986); M. Falk, J. Chem. Phys. **86**, 560 (1987).

[15] R. M. Marsolais, M. Michaud, and L. Sanche, Phys. Rev. A **35**, 607 (1987).

[16] P. J. Chantry, J. Chem. Phys. **57**, 3180 (1972).

[17] G. J. Schulz, Phys. Rev. **128**, 178 (1962).

[18] D. Rapp and D.D. Briglia, J. Chem. Phys. **43**, 1480 (1965).

[19] O.J. Orient and S. K. Srivastava, Chem. Phys. Letters **96**, 681 (1983); S. K. Srivastava and O.J. Orient, Physical Review A **27**, 1210 (1983).

[20] A. Stamatovic and G.J. Schulz, Phys. Rev. A **7**, 589 (1973).

[21] R. Abouaf, R. Papineau, and F. Fiquet-Fayard, J. Phys. B **9**, 303 (1976).

[22] R. Dressler and M. Allan, Chem Phys. **92**, 449 (1985).

[23] C. R. Claydon, G. A. Segal, and H. S. Taylor, J. Chem. Phys. **52**, 3387 (1970).

[24] G.J.Schulz and D. Spence, Phys. Rev. Letters **52** (1969).

[25] D.C. Cartwright and S. Trajmar, J. Phys. B **29**, 1549 (1996).

[26] M. Tronc, R. Azria, Y. Le Coat, P. Cloutier, and L. Sanche, Chem. Phys. **254**, 69 (2000).

[27] I. Koyano, T.S. Wauchop, and K.H. Welge, J. Chem. Phys. 63, 110 (1975).

[28] L.R. LeClair and J.W. McConkey, J. Phys. B **27**, 4039 (1994).

[29] M.-J. Hubin-Franskin, J. Delwiche, B. Leclerc, and D. Roy, J. Phys. B **21**, 3211 (1988).

[30] Y. Itikawa, J. Phys. Chem. Ref. Data **31**, 749 (2002).

[31] The threshold energy is calculated with the energy to dissociate $CO_2$ into O and CO (*i.e.,* 5.451eV) from Ref. 30, and the ionization energy of O (*i.e.,* 13.618 eV).

[32] R. Locht and M. Davister, Int. J. Mass Spectrom. Ion Processes **144**, 105 (1995).

[33] R. Locht, Int. J. Mass Spectrom. Ion Processes **148**, L17 (1995).

[34] N. Bussieres and P. Marmet, Can. J. Phys. **55**, 1889 (1977).

[35] K. E. McCulloh, J. Chem. Phys. 59, 4250 (1973).

[36] J.H.D. Eland and J. Berkowitz, J. Chem. Phys. 67, 2782 (1977).

[37] C. Tian, C.R. Vidal, Phys. Rev. A 58, 3783 (1998).

II. 3. ARTICLE no 3 : Bond Formation in Reactions of Solid Cyclopropane Induced by Low-Energy Electrons

Swiderek, P., Deschamps, M. C., Michaud, M., & Sanche, L. (2003). Bond Formation in Reactions of Solid Cyclopropane Induced by Low-Energy Electrons. *The Journal of Physical Chemistry B*, *107*(2), 563-567. https://doi.org/10.1021/jp021695o

II. 4. ARTICLE no 4 : Absolute cross sections for the electron-induced isomerisation of cyclopropane to propene in the condensed phase

# Absolute cross sections for the electron-induced isomerisation of cyclopropane to propene in the condensed phase

**Petra Swiderek,**

*Institut für Physikalische Chemie II, Universität zu Köln, Luxemburger Str. 116, 50939 Köln, Germany*

**Mathieu C. Deschamps, Marc Michaud, and Léon Sanche**

*Groupe des Instituts de Recherche en Santé du Canada en Sciences des Radiations, Faculté de Médecine, Université de Sherbrooke, Sherbrooke, Québec, Canada J1H 5N4*

## Abstract

Electron-stimulated reactions in solid films of cyclopropane, condensed on an Ar spacer deposited on a Pt substrate, were induced and monitored simultaneously using a high-resolution electron energy loss spectrometer. Absolute cross sections for the formation of propene, including similar unsaturated species, were determined as $\sigma_p = (7.2 \pm 3.9) \times 10^{-17}$ cm$^2$ and $\sigma_p = (9.6 \pm 4.8) \times 10^{-17}$ cm$^2$ at an incident electron energy of 15 eV using both characteristic electronic and vibrational energy losses respectively. The cross section obtained as a function of the film thickness of cyclopropane deposited on a fixed 5-layer spacer of Ar was found to increase above 3-layer coverage. This suggests that intermolecular reactions are not only involved, but also increase the production rate of unsaturated compounds in multilayer films. Quenching of the reaction by the Pt surface, on the other hand, can be excluded because the production rate in a monolayer film of cyclopropane was found to be constant as function of the thickness of the underlying Ar spacer.

## 1. Introduction

Chemical reactions induced by low-energy electrons are not only important as fundamental steps of processes following the production of secondary electrons under the effect of high-energy radiation /1/. They are also interesting as a tool for modifying or patterning surfaces of molecular materials such as ultrathin organic coatings. This concerns not only plasma processes /2/ but can also be done on a macroscopic scale by rastering the surface with a focussed beam of electrons /3/, exposing it to electrons through a mask /4/, or on a nanometer scale by using the tip of a scanning tunneling microscope as a local electron source /5/. Although examples of such modifications are known, the reaction mechanisms are far from being understood. Therefore fundamental studies concerning the products and cross sections of elementary reaction steps taking place at or near the surface of ultrathin molecular films under exposure to low-energy electrons are required.

Since the cross sections for low-energy electron-induced reactions may vary strongly with electron impact energy ($E_0$), it is of utmost importance to study these reactions at well-defined $E_0$. Given these cross sections and the knowledge of the energy distribution of secondary electrons, for instance, would make it possible to assess modifications to a sample upon high-energy irradiation. High-resolution electron-energy-loss (HREEL) spectroscopy can be used both for sample irradiation at a chosen $E_0$ and analysis of the modifications at the same time. This provides an important advantage over XPS, which is a convenient method to follow modifications in the immediate chemical environment of specific atoms /6/ but itself may induce fast and unspecific sample

damages due to the use of high-energy radiation. Compared to temperature programmed desorption (TPD), which is frequently used to investigate electron-induced reactions /7/, but may involve thermally activated secondary processes, HREEL spectroscopy offers the advantage that temperature changes are not required to monitor the products. In addition, vibrational and electronic excitations can both be detected without modification of the experimental arrangement /8,9/. The former excitations reveal fingerprints of specific molecular subunits, whereas the latter are most valuable for the identification of the type of $\pi$-electron system present in the reaction products.

In the present work, we use the combination of vibrational and electronic spectroscopy to study in more detail the electron-induced isomerization of cyclopropane to propene. This reaction was identified recently as an initial step in the modifications of solid multilayer films of cyclopropane exposed to sub-nanoampere currents for extended times /9,10/. Interestingly, electron-induced reactions have not been detected at such low incident currents in the case of cyclopropane adsorbed at monolayer coverage on Cu(110) /11/. These findings suggest that multilayer films of cyclopropane are more reactive under exposure to low-energy electrons. The aim of the present study is to quantify the reactivity by measuring the cross section for the production of propene at $E_0 = 15$ eV. A method for measuring absolute cross sections for electron-induced reactions in the condensed phase has been established previously for the case of CO formation from different oxygen containing molecules /12,13/. The same approach serves here to determine the cross section for the isomerization of cyclopropane. Characteristic signals of the product propene in both the vibrational and electronic excitation ranges are used to quantify its formation.

The suspected low reactivity of cyclopropane at monolayer coverage has been ascribed to either a stabilisation of the intermediate radicals through binding to the metal surface /14/ or may simply result from quenching of an excitation or a resonance that would otherwise lead to a reaction /15/. Furthermore, contributions of intermolecular reactions should be favored at multilayer coverage because of the larger number of immediate neighbors. To evaluate the importance of these effects, we have investigated the production of propene as a function of both the thickness of the cyclopropane film and that of a spacer film of Ar, which is generally used to suppress possible effects of the underlying Pt(111) substrate. The present results are compared to and discussed in the context of the previous results for monolayer cyclopropane on Cu(110) /11,14/.

## 2. Experiment

The experiments were performed with an electrostatic HREEL spectrometer described in detail previously /16/. Briefly, the spectrometer consists of a monochromator and an analyzer both having hemispherical deflectors with rectangular entrance and exit slits. Double zoom lenses at the exit of the monochromator and at the entrance of the analyzer allow a nearly constant beam focussing and beam size over the electron energy range 2 - 25 eV. The monochromator, which can be rotated from 8° to 80° with respect to the normal of the sample, was set at 15° and the analyser fixed at 45° at the opposite azimuth. The incident energy scale ($E_0$) was calibrated to ±0.1 eV using the onset of the current transmitted through the sample. The combined resolution of the spectrometer was

set at 16 meV full width at half maximum for a current $I_0 = 0.18$ nA incident on the sample surface. The apparatus is housed in a μ-metal UHV chamber that is maintained at a base pressure of $10^{-10}$ Torr by the combined action of a 400 l/s ion pump and a liquid-$N_2$ cooled titanium sublimation pump.

The samples are initially prepared from the gas phase using a gas-handling manifold. Known amounts of gas, measured from the differential pressure drop in a calibrated volume, are leaked via a stainless steel capillary having an opening located just in front of a Pt(111) single crystal (Johnson and Matthey). The crystal is mounted on a low-temperature sample manipulator that allows cooling down to 18 K, precise translations in the X, Y, and Z directions, as well as azimuthal and flip rotations, as described in detail previously /17/. This device enables a determination of the incident beam profile via measurement of the spatial distribution of the products formed when the sample is exposed to electrons. The surface of the crystal was cleaned by resistive heating. Cyclopropane was purchased from Aldrich at a stated purity of 99+% and propene from Matheson at a stated purity of 99.6%. The molecular films were condensed on spacer films of argon (99.9995%, Matheson of Canada Ltd.) of variable thichnesses to study the effect of distance from the Pt surface. The number of layers in a condensed film was estimated to ±10% from the calibrated amount of gas needed to deposit a monolayer, assuming no change in sticking coefficient and growth mode for the adlayers, as described elsewhere /18/. The reliability of this estimate was further verified by monitoring the transmitted current before and after each film deposition.

## 3. Results

### *a) Energy loss spectra*

Vibrational HREEL spectra of a 5-layer film of cyclopropane deposited on a 5-layer spacer of Ar after a brief and after a prolonged exposure to 15-eV electrons are shown in Fig. 1. At this energy the production of propene is easily detected as shown previously /9,10/. To measure the production rate, several vibrational spectra were recorded in sequence with the electron beam focussed at the same location on a film. The probed part of the film was thus exposed to electrons having a constant incident energy during the entire experiment. As a result, each spectrum contains information that is averaged over its acquisition time, which is reported in Fig. 1. Production of propene is obvious from characteristic changes in the vibrational spectrum during exposure to the electron beam. Briefly, the intensity between 170 meV and 180 meV increases and a shoulder appears around 200 meV. This latter signal stems from the excitation of the C=C stretching vibration as supported by the comparison with a spectrum of a pure propene film (Fig. 1 and ref. 10). The CH stretching peak (380 meV) broadens considerably and decreases in height during exposure, implying that a part of the original intensity is shifted towards lower energy loss. This is again consistent with the formation of propene as evident from a typical saturated CH stretching band at lower energy loss (≈360 meV). The shoulder appearing on the low-energy side of the CH stretching band, upon formation of propene, is the easiest to quantify among the vibrational signals. The evolution of the integral intensity in the range between 339 and 362 meV (marked by vertical dashed lines in Fig. 1) will therefore be used for the determination of the propene production rate.

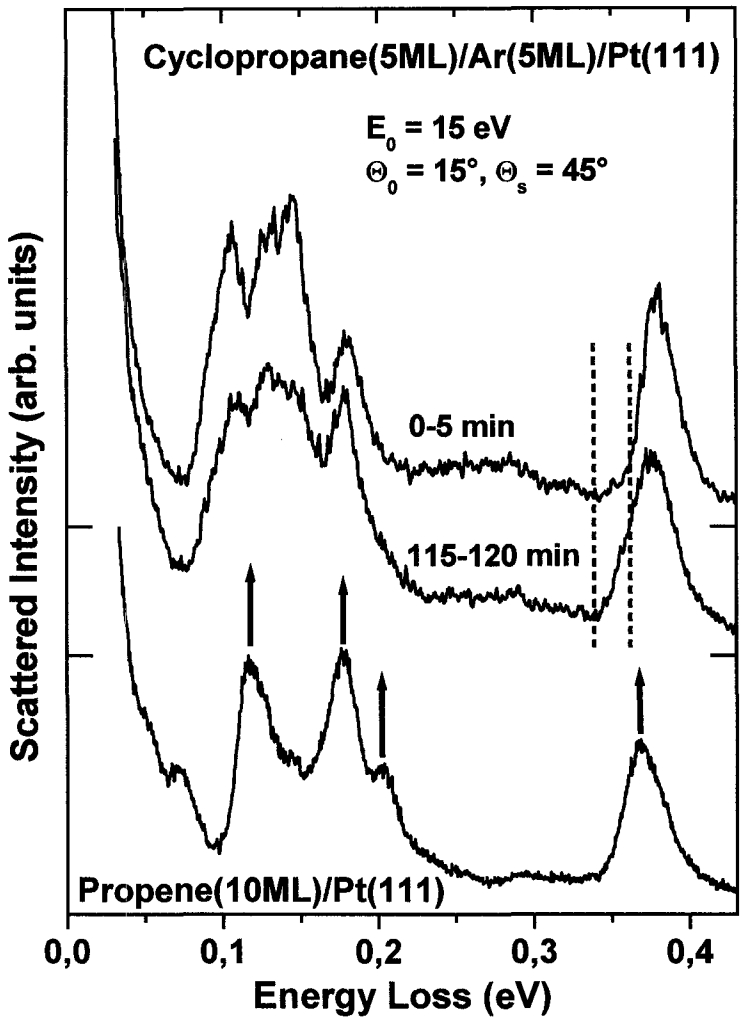


Fig.1 Vibrational electron energy loss spectra of a 5-layer cyclopropane film on a 5-layer spacer of Ar recorded at $E_0$ = 15 eV for the first 5 min interval of electron exposure and for a 5 min interval after about 2 h of exposure. For comparison, the spectrum of a 10-layer film of propene recorded for the first 5 min interval of electron exposure at the same $E_0$ is included. Vertical dashed lines indicate the range over which the spectra of the reaction mixture are integrated for the quantitative measurement of propene formation. (ML = monolayer equivalent). The short horizontal bars indicate the zero base line of the vertically shifted spectra.

Electronic HREEL spectra recorded for different time intervals during electron exposure of a 5-layer film of cyclopropane deposited on a 5-layer spacer of Ar at $E_0$ = 15 eV are shown in Fig. 2. Curve (a) results from a sum of 26 recordings of 2-min acquisition time, each of which was taken on a fresh sample or at a new (X,Y) position on a locally exposed sample. Such a sum of data is representative of a spectrum in the limit of a short irradiation time. It is therefore largely free of reaction products and compares closely to the very broad and structureless optical spectrum of solid cyclopropane /19/. For a longer acquisition time noticeable changes appear in the spectrum, as one can see in Fig. 2(b). The most important one is the appearance of a new excitation on the low-energy side of the original cyclopropane band with an onset at about 6.4 eV. This band is attributed to the $^1\pi\pi^*$ transition of propene as shown previously /9/. In addition, two bands located around 4.3 eV and 5.3 eV become obvious. The lowest-energy one is assigned to the $^3\pi\pi^*$ transition of propene /9,20/, while the higher one is due to a secondary reaction product containing a conjugated diene unit /9/. In this work, propene formation is quantified from the evolution of the $^3\pi\pi^*$ transition in the HREEL spectrum recorded at $E_0$ = 15 eV during exposure to 15-eV electrons.

***b) Dependence of the electronic spectrum on the electron exposure and cross section calibration***

The amount of propene produced by 15-eV electrons incident on the cyclopropane film deposited on a 5-layer spacer of Ar, as probed from the integral intensity of the $^3\pi\pi^*$ excitation of propene between energy losses of 4.2 and 4.7 eV (vertical dashed lines in

Fig. 2), is shown as a function of the exposure time in Fig. 3. During at least the first 20 min of bombardement the intensity of the signal increases linearly. This indicates that during the initial stages of the product formation the reaction rate is practically constant and charging effects are minimal.

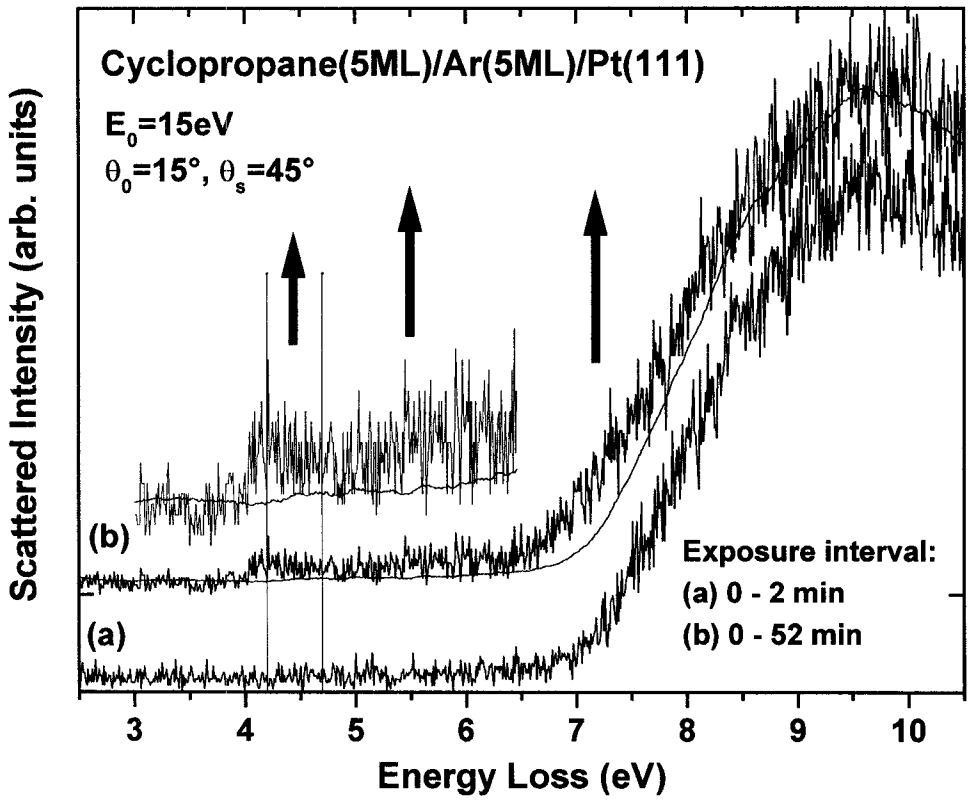


Fig.2 Representative electron energy loss spectra of a 5-layer film of cyclopropane on a 5-layer spacer of Ar recorded at $E_0$ = 15 eV. (a) Sum of 26 spectra each obtained for 2-min exposure time either on a fresh sample or at a new beam location on the same sample, (b) spectrum obtained on the same sample and location during an exposure interval from 0 to 52 min. The mean spectrum of (a) is reproduced for comparison. Vertical dashed lines indicate the range over which the spectra of the reaction mixture are integrated during the experiments aiming at the quantitative measurement of propene formation. (ML = monolayer equivalent). The short horizontal bars indicate the zero base line of the vertically shifted spectrum.

Within this linear reaction regime, the slope of a straight line passing through the experimental data represents, within a constant factor, the production rate (in counts per min) of only those molecules that can be *detected* by the probing electron beam. Here and in the following, we will refer to this quantity as an *apparent* production rate as opposed to the *actual* amount of molecules produced per unit time. To determine the constant factor and thus quantify the production rate, cyclopropane films containing up to 8% of propene (i.e. reference mixtures) and having identical thicknesses as those for the bombardment experiments were deposited on 5-layer spacers of Ar and their spectra recorded. The integral intensities of the $^3\pi\pi^*$ transition of propene in the reference mixtures, shown as solid triangles in Fig. 3, exhibit an almost linear increase with propene concentration, which is given in % on the top scale. By aligning the reference mixture data to the straight line obtained from a fit to the electron exposure data (open circles and bottom scale in Fig. 3), we obtain the calibrated production rate of propene as being $(0.40 \pm 0.08)\%\cdot\text{min}^{-1}$ at $E_0 = 15$ eV. From this value an *absolute* electron scattering cross section $\sigma_p$ for the formation of propene can be determined with the method described previously /12,13/. Assuming for simplicity an incident electron beam characterized by a constant current density $i_0 = I_0 / S_0$ within the beam area $S_0$ and $i_0 = 0$ outside, we obtain the cross section from the relation

$$\sigma_p \cong \frac{n_{\text{Propene}} S_0}{n_0 I_0 t} \qquad (1)$$

In this expression, $n_0$ represents the number density of molecules in the film prior to bombardment (i.e. the number density of cyclopropane in the fresh film) and $n_{\text{Propene}}$ the number density of propene molecules formed after a bombardment time $t$. The calibrated

production rate corresponds to the combined factor $n_{Propene}/n_0 \cdot t$, that derives from the relation between the propene signal intensity and the concentration of propene in a mixture film (Fig. 3). $S_0$ was determined in a different bombardment experiment from the profiles in the X and Y directions of the intensity of the CH stretching signal of propene integrated over the range specified in Fig. 1. The resulting triangular intensity profiles in both directions, which are similar to those obtained in ref. 12, indicate a practically constant current density over the irradiated area $S_0 = (1.2 \pm 0.2) \times 10^{-3}$ cm$^2$. Finally, taking $I_0 = (0.18 \pm 0.04)$ nA, we find a cross section $\sigma_p = (7.2 \pm 3.9) \times 10^{-17}$ cm$^2$ at $E_0 = 15$ eV.

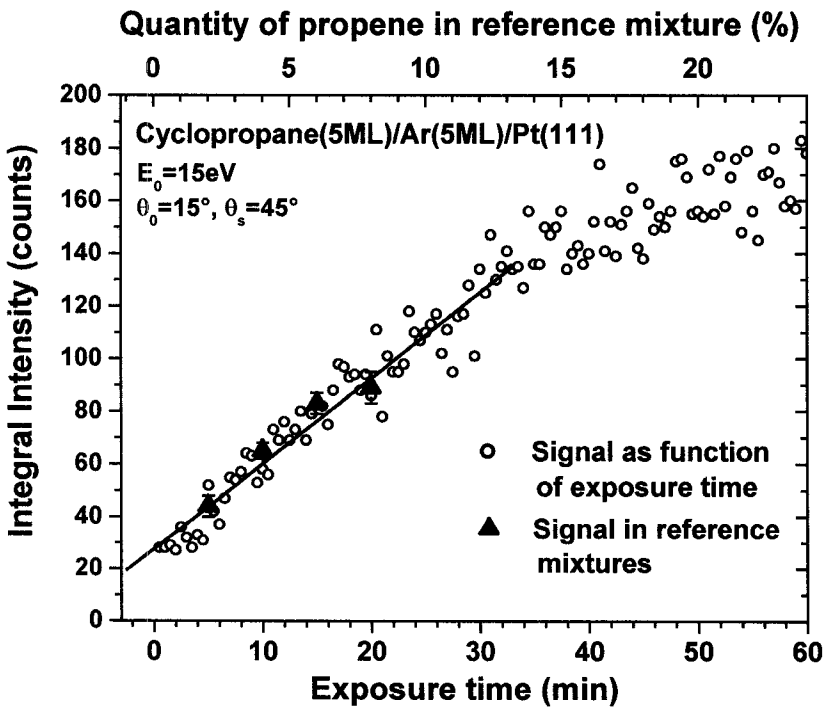


Fig.3 Integral intensity (O) between 4.2 and 4.7 eV, (i.e., in the range of the lowest triplet band of propene as indicated in Fig. 2), during exposure of a 5-layer film of cyclopropane deposited on a 5-layer spacer of Ar to 15-eV electrons. Integral intensity (▲) in the same spectral range recorded at $E_0 = 15$ eV on 5-layer films of reference mixtures deposited on 5-layer spacers of Ar plotted as a function of propene content as given on the top scale. The solid line represents a linear fit to the

data of the exposure experiment during the initial 20 min of exposure. (ML = monolayer equivalent).

### *c) Dependence of the vibrational spectrum on the electron exposure and cross section calibration*

The cross section for the formation of propene from cyclopropane can also be determined from an analysis of vibrational energy losses. Here using the CH stretching signal of propene integrated over the range indicated in Fig. 1, we determine this cross section from a 5-layer film of cyclopropane deposited onto a 5-layer spacer of Ar at $E_0$ = 15 eV. Again, as one can see in Fig. 4, the intensity of this signal increases linearly during at least the first 20 min. As for the case of the $^3\pi\pi^*$ excitation, the slope of the straight line resulting from a fit within the linear regime yields an apparent production rate. Comparing this production rate from two exposure experiments to the dependence of the integral CH signal on the propene concentration in several reference mixtures, we deduce an average calibrated production rate of (0.59±0.15)%·min$^{-1}$. Owing to intensity fluctuations among the vibrational spectra, this comparison is based on intensities relative to the height of the cyclopropane CH stretching band. Taking this calibrated production rate, the average value of the measured irradiated area for the two experiments $S_0 = (1.1 \pm 0.2) \times 10^{-3}$ cm$^2$, and the incident current $I_0 = (0.18 \pm 0.04)$ nA, we obtain a cross section of $\sigma_p = (9.6 \pm 4.8) \times 10^{-17}$ cm$^2$ at $E_0$ = 15 eV.

Experiments on the changes in the vibrational HREEL spectra were performed for different cyclopropane and Ar film thicknesses. Because of a relatively large scatter in the intensity data of the reference mixture films at monolayer coverage the cross section was determined only for multilayer films of cyclopropane. Such a scatter in the intensity data

can be traced back to slight variations in the quality of the underlying Ar spacers, which leads to sizeable changes in the phonon background intensity especially in the range of weak vibrational signals. Nonetheless, relative values in terms of the apparent production rate (in counts/min), can still be used to compare the reaction rate under different conditions, including those which are not accessible to the determination of an absolute value. This procedure is applied in the next section.

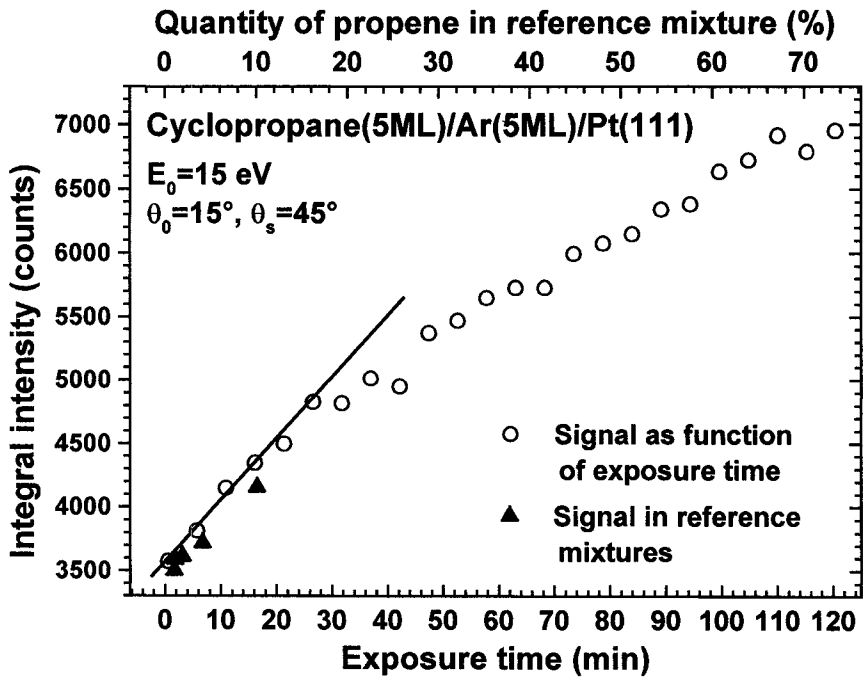


Fig.4 Integral intensity (O) between 0.339 and 0.362 eV, (i.e., in the range of the CH stretching band of propene as indicated in Fig. 1), during exposure of a 5-layer film of cyclopropane deposited on a 5-layer spacer of Ar to 15-eV electrons. Integral intensity (▲) in the same spectral range recorded at $E_0$ = 15 eV on 5-layer films of reference mixtures deposited on 5-layer spacers of Ar as a function of propene content as given on the top scale. The solid line represents a linear fit to the data of the exposure experiment during the initial 20 min of exposure. (ML = monolayer equivalent).

***d) Dependence of the propene production on cyclopropane coverage and Ar-spacer thickness***

In Fig. 5(a) we show the apparent production rate in terms of the CH stretching signal ascribed to propene (Fig.1) as a function of the cyclopropane coverage on a 5-layer spacer of Ar. In Fig. 5(b), we show the corresponding cross section for propene production as obtained from comparing to the multilayer reference mixtures and using Eq. 1. This result should give information more specifically on the importance of possible intermolecular reaction steps. In Fig. 6 we show the apparent production rate for a fixed monolayer coverage of cyclopropane deposited on a variable spacer thickness of Ar. This should reveal if a quenching process involving electron or energy transfer from the cyclopropane to the metal surface could reduce the reaction rate.

Assuming small electron exposures, negligible electron beam attenuation within a film, and single electron-molecule collisions with no further reaction of the initial molecular product with its neighbors, the production rate should be constant with time and directly proportional to the number of irradiated molecules /12,13/. This has been found to be the case for the production rate of CO in acetone films over the thickness range 0 - 5 layers /12/ and in methanol films over the range 0 - 12 layers /13/ from probing the $d^3\Pi$ electronic excitation of CO in those films. However, in Fig. 5 the apparent production rate at large film thicknesses is found to deviate slightly to higher values from the linear extrapolation (dashed line) based on the values at one and two layer. This immediately suggests that the reaction proceeds at a faster pace in the multilayer regime. This also agrees with a previous qualitative work where the spectral changes have been found to be much more prominent in a multilayer film of cyclopropane than at monolayer coverage

/8/. If the percentage of propene formed in the cyclopropane film during a given electron exposure would have been independent of the film thickness then the relative intensities of propene and cyclopropane signals would have been the same irrespective of thickness. This larger probability of propene formation in the multilayer film can be better corroborated by the plot of the corresponding cross section values in Fig. 5 (b). Under the assumption of single electron-molecule collisions these values should be independent of the film thickness even in presence of electron-beam attenuation. This is found to be the case at 2 and 3 layers of cyclopropane but not at 5 layers where the cross section increases.

The apparent production rate of propene measured in the variable spacer experiments does not exhibit a marked dependence on the distance to the Pt(111) surface (Fig. 6). Even more, it is not reduced at all in close vicinity to the Pt surface. This indicates that quenching by the metal surface is not effective in the present experiment.

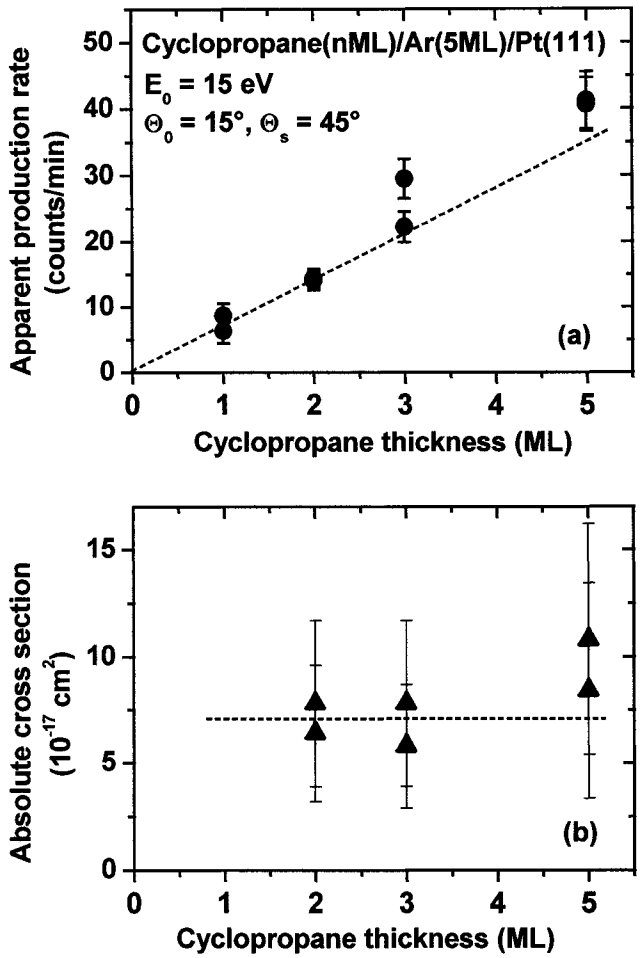


Fig.5 (a) Apparent production rate of propene in cyclopropane films of variable thicknesses deposited on a 5-layer spacer of Ar upon exposure to 15 eV electrons. The amount of propene in a cyclopropene film is monitored in terms of its integrated CH stretching signal in the range defined in Fig.1. The dashed line represents an approximate linear fit to the data points at low thickness as discussed in the text. (b) Absolute cross section for propene formation in cyclopropane films of variable thicknesses. The dashed line serves as guide to the eye. (ML = monolayer equivalent).

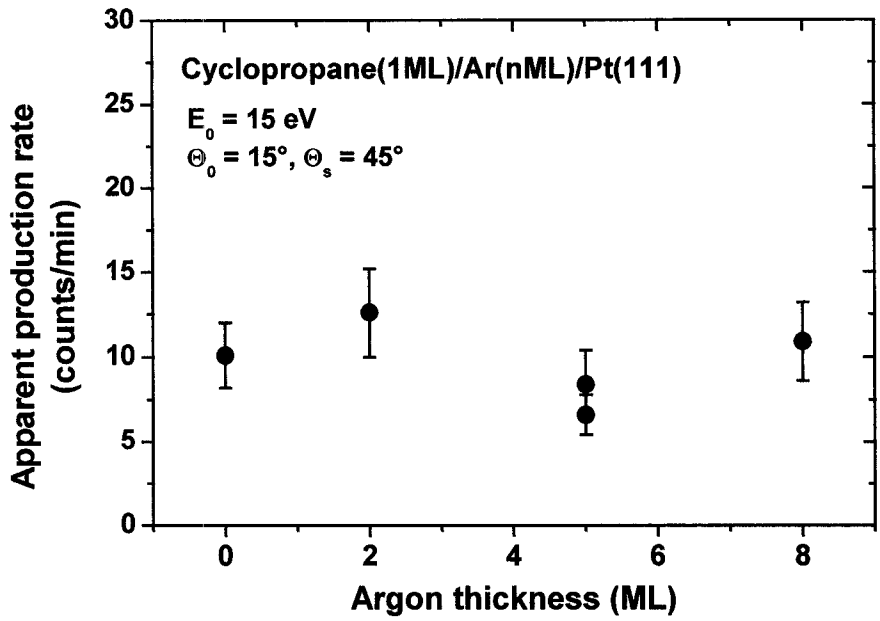


Fig.6 Apparent production rate of propene in a fixed monolayer coverage of cyclopropane deposited on a variable spacer of Ar, upon exposure to 15 eV electrons. The amount of propene is monitored in terms of its integrated CH stretching signal in the range defined in Fig. 1 (ML = monolayer equivalent).

### *e) Effect of the electron beam attenuation*

In addition to possible changes in the reaction mechanism, a discussion of the measured production rate must take into account the attenuation of the probing electron beam within the solid. For electrons that enter, scatter once on specific molecules, and then leave the film, thus generating a backscattered signal, the *probed depth* corresponds to half of the average of the electron mean free paths at the initial and final electron energies. This effect limits the distance within which the newly formed molecules in a solid film can be probed or detected efficiently. Also, this is what makes the measured

production rate an apparent quantity. To illustrate this effect, the integral of the energy-loss intensities of the CH stretching signal for 2.5-eV electrons incident on a cyclopropane film is shown as a function of the film thickness in Fig.7(a). The signal follows a linear behavior up to a coverage of about two layers and then reaches a saturation level at higher coverages.

The same is found for the thickness dependence of the energy-loss integral of the CH stretching signal for 15-eV electrons incident on a pure cyclopropane film and reference mixture films containing 10% propene as shown in Fig. 7(b). In the mixture case, the energy-loss integrals are included for both the propene CH signal between 340 - 362 meV (i.e., in a range similar to that used for the determination of production rates) and the cyclopropane CH signal between 370 - 420 meV. In the cyclopropane case, the energy-loss integral was extended over the whole CH stretching signal (i.e. 348 – 421 meV). Corresponding values for the integrated signals at zero coverage in Fig. 7(b) were obtained simply from the line passing across the base of the CH stretching peak for the monolayer coverage. Judging from the tendancy to saturation of the CH stretching signal at coverages above two layers, the apparent production rate would indeed underestimate the total amount of propene owing to the corresponding limited *probed depth* for vibrations. In other words, as mostly the outer layers of the cyclopropane film are effectively probed, the observed intensity increase upon electron exposure reflects essentially the amount of propene formed within these layers. A comparison of apparent production rates for different film thicknesses as reported in Fig. 5(a), therefore, has to take into account the limited *probed depth* within the cyclopropane film. On the contrary, the absolute cross sections reported in Fig. 5(b) are not subject to the same limitation.

This effect cancels out when the apparent production rate in a given film is divided by the slope of the straight line passing through the intensities of the reference mixtures plotted as function of propene percentage in a film of same thickness because both measurements probe the same number of layers.

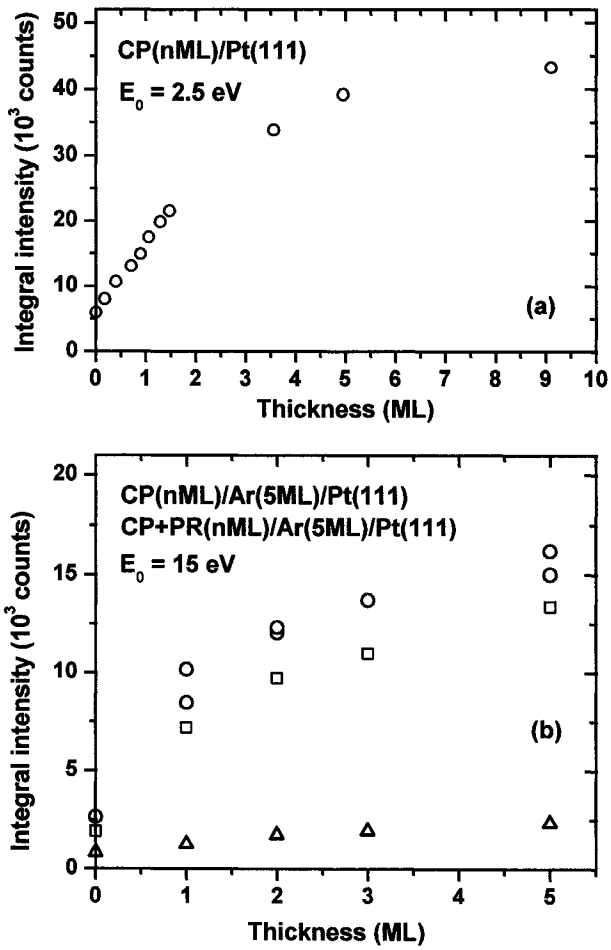


Fig.7 (a) Integral CH stretching intensities in the range between 348 and 421 meV as function of film thickness at $E_0 = 2.5$ eV for cyclopropane (CP) deposited on Pt(111). (b) Integral CH stretching intensities at $E_0 = 15$ eV as function of film thickness for both cyclopropane (O 348-421 meV) and a reference mixture containing 90% cyclopropane and 10% propene (CP+PR) (□ 370-420 meV, Δ 340-362 meV) deposited on a 5-layer spacer of Ar (b). Electrons were incident at an angle of 15° and detected at 45°. (ML = monolayer equivalent).

## 4. Discussion

### *a) Cross sections*

The cross sections for electron-induced production of propene in cyclopropane at an incident energy of $E_0 = 15$ eV as obtained independently from the electronic and vibrational spectra agree reasonably well. It is interesting to compare the present values with that obtained in a previous study on electron-induced reactions of cyclopropane adsorbed at monolayer coverage on Cu(110) cooled at 90 K /14/. In that work a much higher current has been used to observe changes in composition of the sample /11/ and the chemisorbed cyclopropyl radical and a metallacyclobutane have been identified as products at $E_0 = 10$ eV /11,14/. A cross section of $\sigma_p = 8\times10^{-18}$ cm$^2$ has been reported for this reaction /14/. A closer examination of the data reported in the same paper suggests that the cross section has been obtained from an analysis of a decreasing cyclopropane signal and should more exactly be considered as a total depletion cross section. On the other hand, if the immediate and only products of the reaction are the two radical species that have been proposed, the same cross section may be attributed to the formation of these species. The mere fact that the reaction was less obvious at $E_0 = 15$ and 18 eV suggested the presence of a resonant mechanism /14/. The finding from TPD experiments that the amount of cyclopropyl was four times that of metallacyclobutane /14/ would imply a cross section of $\sigma_p = 6.4\times10^{-18}$ cm$^2$ for the formation of the former. This is an order of magnitude smaller than the present values for formation of propene. This explains why the product on Cu(110) was so difficult to detect at typical subnanoampere current /11/. Another factor that contributes to this problem is the area irradiated by the incident electron beam. In the monolayer study on Cu(110) this area was 0.02 cm$^2$, which

is more than an order of magnitude larger than the present one. As a result, the rate of product formation must have been accordingly slower owing essentially to the smaller incident current density.

In the study of cyclopropane on Cu(110) the sample has been exposed to about $10^{17}$ $e^{-}\cdot cm^{-2}$ before the analysis of the products /14/. This is two orders of magnitude larger than the present electron exposure during the first 20 min and which leads to the formation of about 10% of the product. As the sample is continuously irradiated, subsequent collisions between the incident electrons and the products, can still be neglected only in this linear regime. Considering the cross section for formation of the radical species on Cu(110) as given above, and assuming that secondary reactions of the radical species are not taking place, the overall production should have approached more than 50% in that experiment. The present experiment avoids such large overall productions because of possible secondary reactions of the immediate products, which are not included in the simple linear treatment of the reaction kinetics.

Another previous study concerns the decomposition of cyclopropane adsorbed on Pt(111) at 100 K, again at monolayer coverage, but under exposure to higher energy electrons with $E_0 = 50$ eV /21/. From the decrease of the parent TPD signal with increasing electron exposure a total depletion cross section of $\sigma_p = 8\times10^{-17}$ $cm^2$ has been deduced. While that value is similar to the present multilayer result, one must keep in mind that at such high energy several reactive inelastic processes yielding unknown species can be initiated by a single electron.

We also have to comment on the exact meaning of the cross sections derived from the present measurement. So far we have assumed that exposure of cyclopropane to low-

energy electrons yields only propene as primary product, (i.e., the product formed after a single electron collision):

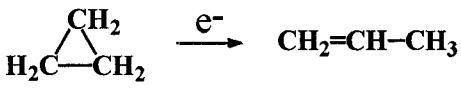

(2)

We have, on the other hand, shown previously that secondary products with higher molecular weight containing a conjugated diene unit are formed upon extended electron exposure /9/. This was explained by radical formation or possible ionization leading to standard oligomerisation reaction steps. Assuming further that H migration along the chain is slow, it was concluded that these latter steps alone could not produce a conjugated oligomer. Additional electron collision processes leading to H abstraction were then invoked for the formation of the conjugated diene units /9/. More specifically, dimers containing two isolated double bonds can arise from two sequential reactions triggered by a single electron collision process as:

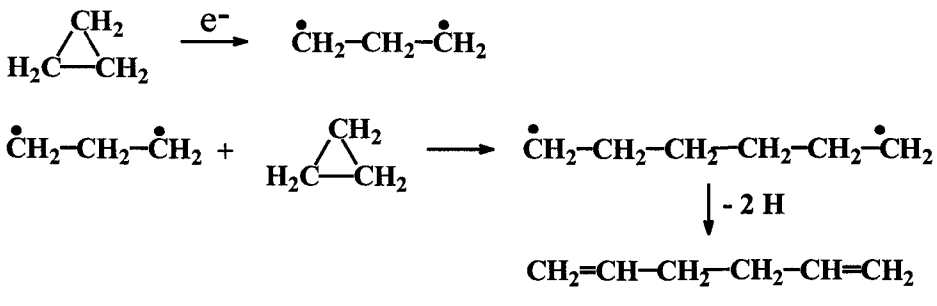

(3a)

(3b)

Such products must have spectroscopic properties (i.e., double bond stretch, saturated CH stretching bands, and triplet states) that are very similar to and therefore not easy to distinguish from those of propene. These additional products could consequently be counted together with the propene signal.

***b) Spacer thickness dependence of the production rate***

Fig. 6 shows that quenching of intermediate reactive species at the metal surface is not effective in the present experiment. Also, a different reaction mechanism would, in analogy to the monolayer results on Cu(110) at 90 K /11,14/, have to be expected for a catalytically active clean metal surface. Therefore, it must be noted that during the present experiments the Pt crystal was cleaned merely by resistive heating. Vibrational HREEL spectra immediately after heating showed small intensity peaks due to the presence of a fractional layer of hydrocarbon residues at the Pt(111) surface. This appears to prevent not only chemisorption that would lead to different reactions under electron impact /11/ but also to effectively screen any long-range quenching process. Such a limited quenching range differs from previous findings concerning the electron-induced dehydrogenation of alkanethiol self-assembled monolayer (SAM) films on gold /15/. In those experiments, dehydrogenation at electron energies around 10 eV, most probably through a resonant mechanism, has been found to be strongly localized near the methyl terminations of the film and its associated cross sections to increase rapidly with chain length (e.g., $1.2\times10^{-16}$ $cm^2$ for the $C_8$ SAM to $5.3\times10^{-16}$ $cm^2$ for the $C_{16}$ SAM). This difference indicates that in SAM films quenching is effective even at some distance from the metal surface. This could result simply from the fact that the molecules are chemically bound to a metal surface in SAM films or else reflects that the lifetimes of the excited states involved in the SAM decomposition and the isomerization of cyclopropane are different.

***c) Increase of the rates of product formation with cyclopropane coverage***

The production of propene or another compound containing isolated double bonds, as probed using the characteristic CH stretching bands, from cyclopropane under exposure to 15-eV electrons is observed to proceed at a faster rate in a multilayer film. As it can be seen in Fig. 5(a) the apparent rate for the 5-layer film is about six times larger than that for the monolayer. However, considering that this production rate is subjected to a *probed depth*, which is limited to about three layers in a cyclopropane film, the increase of the production rate must be considered to be even higher.

The above finding together with the result that quenching is not effective suggests that neighboring molecules must be responsible for this increase of the cross section. Initially, the concentration of propene is sufficiently small to consider only cyclopropane molecules to influence the production rate at multilayer coverage. A possible scenario describing the initial physico-chemical processes involves the two parallel reactions (2) and (3) described in Section 4.*a*. While the formation of the diradical (3a) may be involved as intermediate in the direct isomerization of cyclopropane to propene (2), the same diradical may also induce the dimerization step (3b) if enough close neighbors are present. An equivalent reaction can be formulated for the case of an ionic mechanism following ionization above 10 eV /19/. If process (3b) is fast enough, a single electron collision could initiate as well the formation of dimers containing two isolated double bonds, both of which having a very similar spectroscopic fingerprint. The reaction mechanism including process (3a) followed by (3b) therefore gives a reasonable explanation for the increased production rate of species with isolated double bonds at multilayer coverage.

## 5. Conclusions

Absolute reaction cross sections for the electron-induced isomerisation of cyclopropane to propene in the condensed phase were determined by HREEL spectroscopy by monitoring both vibrational and electronic excitations of propene. The cross sections include the formation of similar unsaturated products with isolated double bonds whose spectral signature cannot be distinguished from propene under the present experimental conditions. The independent measurements of the absolute cross sections obtained for a 5-layer film of cyclopropane at an incident energy of 15 eV from the lowest triplet band and the saturated CH stretching signal of propene agree within the present experimental uncertainty. The present values are larger than those obtained from to a previous study on cyclopropane adsorbed onto Cu(110) at monolayer coverage /14/ but are comparable to a total depletion cross section for monolayer cyclopropane on Pt(111) at 50 eV /21/.

A comparison of cross sections for the electron-induced production of propene in cyclopropane films of varying thickness confirms that the reaction rate increases slightly at larger film thickness. This is explained by additional contributions from a second reaction channel that becomes accessible as the number of nearest neighbors increases in the film. This channel leads to the formation of dimers with two isolated double bonds that have a spectroscopic pattern very similar to propene. From the comparison of reaction rates for a monolayer of cyclopropane deposited on an Ar spacer of varying thickness, quenching by the metal surface, on the other hand, does not contribute to the observed decrease of the reaction rate in the monolayer. This is at least partly attributed to the

presence of a very thin hydrocarbon residue on the Pt(111) surface during the present experiments that could not be removed simply by resistive heating.

**Acknowledgements**

This work was sponsored by the Canadian Institutes of Health Research and the German Fonds der Chemischen Industrie.

**References**

/1/ B. Boudaïffa, P. Cloutier, D. Hunting, M. A. Huels, and L. Sanche, Science **287**, 1658 (2000).

/2/ H. Tanaka and M. Inokuti, Adv. At. Mol. Opt. Phys. **43**, 1 (2000).

/3/ W. Geyer, V. Stadler, W. Eck, M. Zharnikov, A. Gölzhäuser, and W. Grunze, Appl. Phys. Lett. **75**, 2401 (1999).

/4/ C. David, H. U. Müller, B. Völkel, and M. Grunze, Microelectronic Engineering **30**, 57 (1996).

/5/ S.-W. Hla, L. Bartels, G. Meyer, and K.-H. Rieder, Phys. Rev. Lett. **85**, 2777 (2000).

/6/ W. Eck, V. Stadler, W. Geyer, M. Zharnikov, A. Gölzhäuser, and M. Grunze, Adv. Mat. **12**, 805 (2000).

/7/ E. D. Pylant, M. J. Hubbard, and J. M. White, J. Phys. Chem. **100**, 15890 (1996).

/8/ P. Swiderek and H. Winterling, Chem. Phys. **229**, 295 (1998).

/9/ P. Swiderek, M. C. Deschamps, M. Michaud, and L. Sanche, J. Phys. Chem. B **107**, 563 (2003).

/10/ H. Winterling, H. Haberkern, and P. Swiderek, Phys. Chem. Chem. Phys. **3**, 4592 (2001).

/11/ R. Martel, A. Rochefort, and P. H. McBreen, J. Am. Chem. Soc. **116**, 5965 (1994).

/12/ M. Lepage, M. Michaud, and L. Sanche, J. Chem. Phys. **113**, 3602 (2000).

/13/ M. Lepage, M. Michaud, and L. Sanche, J. Chem. Phys. **107**, 3478 (1997).

/14/ R. Martel and P. H. McBreen, J. Chem. Phys. **107**, 8619 (1997).

/15/ C. Olsen and P. A. Rowntree, J. Chem. Phys. **108**, 3750 (1998).

/16/ L. Sanche and M. Michaud, Phys. Rev. B **30**, 6078 (1984).

/17/ M. Michaud, P. Cloutier, and L. Sanche, Rev. Sci. Instrum. **66**, 2661 (1995).

/18/ L. Sanche, J. Chem. Phys. **71**, 4860 (1979).

/19/ H. Basch, M. B. Robin, N. A. Kuebler, C. Baker, and D. W. Turner, J. Chem. Phys. **51**, 52 (1969).

/20/ A. Kuppermann, W. M. Flicker, and O. A. Mosher, Chem. Rev. **79**, 77 (1979).

/21/ T. B. Scoggins, H. Ihm, Y. M. Sun, and J. M. White, J. Phys. Chem. B **103**, 6791 (1999).

# III. DISCUSSION ET CONCLUSION

## III.1. SPECTROSCOPIE ÉLECTRONIQUE PAR PERTES D'ÉNERGIE.

La spectroscopie électronique par pertes d'énergie est une technique utilisée efficacement depuis un bon nombre d'années. Toutefois, la grande majorité des travaux réalisés avec cette technique ont jusqu'à maintenant été accomplis en phase gazeuse. Or l'étude des modes de vibrations et des états électroniques d'une molécule en phase condensée peut apporter des informations supplémentaires pertinentes à la compréhension de la molécule. L'étude des états électroniques du $CO_2$ en phase condensée témoigne bien de plusieurs modifications observées dans les états électroniques entre le gaz et le solide. Par exemple, sous l'effet de la polarisation du milieu, les états électroniques ayant un caractère de type Rydberg sont généralement déplacés vers les plus hautes énergies ou disparaissent complètement du spectre alors que les états de type valence peuvent être déplacés vers les plus basses énergies.

Comme certains états électroniques peuvent être très près les uns des autres, ils peuvent être très difficiles à distinguer. Dans certains cas aussi, ils peuvent interagir entre eux afin de se repousser les uns les autres (*avoided crossing*). Le fait de passer à la phase condensée peut permettre de séparer certains de ces états et aussi éliminer certains effets de répulsion.

Ainsi, en modifiant le caractère et la position en énergie de certaines transitions électroniques, les expériences en phase condensée permettent d'obtenir des informations supplémentaires pour l'assignation des états électroniques et offrent en conséquence une compréhension plus complète de la molécule. De plus, l'utilisation de la phase condensée

ouvre la porte à l'étude spectroscopique d'un éventail de nouvelles molécules impossibles à étudier en phase gazeuse sans risque d'altération de la molécule.

## III.2. DÉTECTION *IN SITU* DE COMPOSÉS NEUTRES ET MESURE DE SECTIONS EFFICACES.

Plusieurs études de la fragmentation moléculaire induite par des électrons de basse énergie ont porté sur les fragments chargés (ions positifs ou négatifs). Ces derniers sont généralement facilement observables à l'aide d'un spectromètre de masse. D'autres techniques permettent l'observation de fragments neutres excités (métastables). Néanmoins, peu d'études ont porté sur la détection de fragments neutres dans leur état fondamental. L'utilisation d'un spectromètre de masse pour détecter les fragments neutres implique généralement l'ionisation des fragments ce qui complexifie l'étude étant donné la possibilité d'induire de nouvelles fragmentations. En phase condensée, les fragments neutres restent souvent piégés dans le film. Leur détection par spectrométrie de masse implique alors l'évaporation du film ce qui peut entraîner une altération supplémentaire des fragments. La technique utilisée dans les recherches présentées ici permet de détecter *in situ* les composés neutres piégés dans le film. C'est une méthode basée sur la spectroscopie d'électrons par pertes d'énergie. Elle tire profit de l'apparition de pertes d'énergie attribuables aux excitations électroniques ou vibrationnelles associées aux composés neutres à étudier. Cette méthode utilise donc un même faisceau d'électrons pour induire les dommages et pour détecter les fragments et composés neutres produits. Cette technique a pour avantage de ne pas exiger de modification thermique de l'échantillon condensé. Toutefois, il faut tenir compte que la simple détection des fragments neutres par des électrons peut entraîner de nouveaux dommages à l'échantillon.

Cette technique avait préalablement été appliquée avec succès à l'étude de la production de CO dans des films minces d'acétone et de méthanol. Le signal du premier état électronique du CO étant intense et présentant une structure caractéristique, ce produit est facilement identifiable. Nous avons donc d'abord appliqué la méthode afin de mesurer la production de CO mais cette fois dans des films de $CO_2$. Ensuite, nous avons étudié les réaction induites dans des films de cyclopropane. Afin d'identifier les produits formés, une étude attentive de l'évolution des pertes d'énergie au niveau des vibrations et au niveau des transitions électroniques a été nécessaire. La formation de propène fut identifiée comme étant la réaction principale. Toutefois, les informations tirées des spectres d'énergie perdue montrent hors de tout doute qu'il y a génération de chaînes moléculaires plus longues. Ces résultats montrent donc non seulement que les EBE peuvent mener à une fragmentation moléculaire mais aussi induire des liens chimiques et donc mener à la formation de molécules plus complexes. Afin de pouvoir identifier des produits d'une telle complexité, la combinaison de l'étude des vibrations et des transitions électroniques est donc prometteuse.

L'évolution de l'intensité des pertes d'énergie associées à un composé neutre donné permet de déterminer un taux de production de ce composé et obtenir la section efficace absolue correspondant à cette production. Afin d'étalonner l'intensité des pertes d'énergie associées au produit neutre, il est toutefois nécessaire de pouvoir préparer des échantillons contenant une quantité connue du composé mélangé au produit initial. Cet aspect peut présenter une limitation technique pour l'étude de certains fragments ou composés pour lesquels un tel mélange serait difficilement réalisable.

REMERCIEMENTS

Je voudrais remercier Dr. Léon Sanche de m'avoir accepté dans son équipe et de m'avoir permis de travailler dans un milieu scientifique stimulant, avec des appareils sophistiqués. Je tiens à le remercier particulièrement pour la latitude et l'autonomie qu'il m'a laissées au cours de mes travaux de recherche et le soutien financier qu'il m'a apporté.

Je veux également souligner l'excellent soutien que M. Marc Michaud m'a offert tout au long de mon programme d'étude. Son aide a été précieuse tant pour la réalisation des expériences que pour la rédaction des articles. Marc, merci pour tout le temps que tu m'as accordé et pour ta minutie et ta rigueur !

Je désire également remercier la Dre Petra Swidereck qui a soumis l'idée du projet sur le cyclopropane et qui est venu d'Allemagne pour le réaliser avec moi. Sa présence et ses idées furent stimulantes et nos discussions enrichissantes.

Un gros merci également à Martin Lepage qui m'a montré le fonctionnement du spectromètre d'électrons et à tous les membres du laboratoire (Luc Parenteau, Pierre Lévesque, Pierre Cloutier, Daniel Robillard) et du département qui m'ont offert un milieu de travail agréable et m'ont dépanné à plus d'une reprise.

Finalement un merci tout spécial à ma famille et amis qui ont su me soutenir et m'écouter tout au long de mes péripéties dans mes travaux de recherche.

RÉFÉRENCES


Abe H. et R. Onaka, *J. Phys. Soc. Jpn.* **53**, 1176 (1984).

Abouaf R., R. Papineau, et F. Fiquet-Fayard, *J. Phys. B* **9**, 303 (1976).

Asmis K.R., M. Allan, O. Schafer, et M. Fülscher, *J. Phys. Chem. A* **101**, 2089 (1997).

Atkins P. W., *Physikalische Chemie,* 2nd ed. (VCH, Weinheim, Germany, 1996).

Bader G., G. Perluzzo, L.G. Caron, et L. Sanche, *Phys. Rev. B* **26**, 6019 (1982).

Basch H., M.B.Robin, N.A.Kuebler, C.Baker, et D.W.Turner, *J.Chem.Phys.* **51**, 52 (1969).

Bhattacharya S.K., J. Savario, et M.H. Thiemens, *Geophysical Research Letters* **27**, 1459 (2000).

Boudaïffa B., P. Cloutier, D. Hunting, M.A. Huels, et L. Sanche, *Science* **287**, 1658 (2000).

Brandrup, J., Immergut, E. H., *Polymer Handbook*, 3rd ed. (Wiley, New York, 1989).

Buenker R. J., M. Honigmann, H.-P. Lieberman, et M. Kimura, *J. Chem. Phys.* **113**, 1046 (2000).

Bussieres N. et P. Marmet, *Can. J. Phys.* **55**, 1889 (1977).

Cartwright D. C., S. Trajmar, W. William, et D. L. Huestis, *Phys. Rev. Lett.* **27**, 704 (1971).

Cartwright D.C. et S. Trajmar, *J. Phys. B* **29**, 1549 (1996).

Chantry P. J., *J. Chem. Phys.* **57**, 3180 (1972).

Christophorou L.G., *Electron-Molecule Interactions and their Applications*, Vol.1 et Vol.2 (Academic, New York, 1984).

Claydon C. R., G. A. Segal, et H. S. Taylor, *J. Chem. Phys.* **52**, 3387 (1970).

Cvejanovic S., J. Jureta, et D. Cvejanovic, *J. Phys. B* **18**, 2541 (1985).

Dance D. F., G. A. Keenan, et I. C. Walker, *J. Chem. Soc. Faraday Trans. II* **74**, 440 (1978).

David C., H.U. Müller, B. Völkel, et M. Grunze, *Microelectronic Engineering* **30**, 57 (1996).

De Meijere A., *Methods of organic chemistry* (Houben-Weyl), Vol. E 17c, Thieme, Stuttgart, 1997.

Dressler R. et M. Allan, *Chem Phys.* **92**, 449 (1985).

Dugal P.-C., M.A. Huels, et L. Sanche, *Radiat. Res.* **151**, 325 (1999).

Eck W., V.Stadler, W.Geyer, M.Zharnikov, A.Gölzhäuser, et M.Grunze, *Adv. Mat.* **12**, 805 (2000).

Eland J.H.D. et J. Berkowitz, *J. Chem. Phys.* **67**, 2782 (1977).

England W. B., *Chem. Phys. Lett.* **78**, 607 (1981).

England W. B. et W. C. Ermler, *J. Chem. Phys.* **70**, 1711 (1979).

England W. B., W. C. Ermler, et A. C. Wahl, *J. Chem. Phys.* **66**, 2336 (1977).

England W. B., B. J. Rosenberg, P. J. Fortune, et A. C. Wahl, *J. Chem. Phys.* **65**, 684 (1976).

Falk M. et P. Seto, *Can. J. Spectrosc.* **31**, 134 (1986)

M. Falk, *J. Chem. Phys.* **86**, 560 (1987).

Geyer W., V. Stadler, W.Eck, M.Zharnikov, A.Gölzhäuser, et W.Grunze, *Appl. Phys. Lett.* **75**, 2401 (1999).

Grebner D., M. Helbig, et S.J. Rentsch, *Phys. Chem.* **99**, 16991 (1995).

Green M. A., P.J.O. Teubner, L. Campbell, M.J. Brunger, M. Hoshino, T. Ishikawa, M. Kitajima, H. Tanaka, Y. Itikawa, M. Kimura, et R. J. Buenker, *J. Phys. B* **35**, 567 (2002).

Hall R. I., A. Chutjian, et S. Trajmar, *J. Phys. B* **6**, L264 (1973).

Henglein A., W.Schnabel, et J.Wendenburg, *Einführung in die Strahlenchemie*, Verlag Chemie, Weinheim, 1969, p. 228f.

Herzberg G., *Electronic Spectra of Polyatomic Molecules* (Van Nostrand, New Jersey, 1966).

Hla S.-W., L. Bartels, G. Meyer, et K.-H. Rieder, *Phys. Rev. Lett.* **85**, 2777 (2000).

Holtzhauer K., C. Cometta-Morini, et J.F.M. Oth, *J. Phys. Org. Chem.* **3**, 219 (1990).

Hubin-Franskin M-J, J. Delwiche, B. Leclerc, et D. Roy, *J. Phys. B* **21**, 3211 (1988).

Huels M. A., A. D. Bass, P. Ayotte, et L. Sanche, *Chem. Phys. Letters* **245**, 387 (1995).

Huels M. A., L. Parenteau, P. Cloutier, et L. Sanche, *J. Chem. Phys.* **103**, 6775 (1995).

Itikawa Y., J. Phys. *Chem. Ref. Data* **31**, 749 (2002).

Jorgensen W. L. et L. Salem, *The Organic Chemist's book of orbitals* (Academic, New York, 1973).

Koyano I., T.S. Wauchop, et K.H. Welge, *J. Chem. Phys.* **63**, 110 (1975).

Kuppermann A., W.M. Flicker, et O.A. Mosher, *Chem. Rev.* **79**, 77 (1979).

Langer J., S. Matt, M. Meinke, P. Tegeder, A. Stamatovic, et E. Illenberger, *J. Chem. Phys.* **113**, 11063 (2000).

LeClair L.R. et J.W. McConkey, *J. Phys. B* **27**, 4039 (1994).

Lee C.-H., C. Winstead, et V. McKoy, *J. Chem. Phys.* **111**, 5056 (1999).

Lepage M., M. Michaud, et L. Sanche, *J. Chem. Phys.* **113**, 3602 (2000).

Lepage M., M. Michaud, et L. Sanche, *J. Chem. Phys.* **107**, 3478 (1997).

Locht R. et M. Davister, *Int. J. Mass Spectrom. Ion Processes* **144**, 105 (1995).

Locht R., *Int. J. Mass Spectrom. Ion Processes* **148**, L17 (1995).

Maier G. et S. Senger, *Angew. Chem.* **106**, 605 (1994).

Marsolais R. M., M. Michaud, et L. Sanche, *Phys. Rev. A* **35**, 607 (1987).

Martel R. et P.H. McBreen, *J. Chem. Phys.* **107**, 8619 (1997).

Martel R., A. Rochefort, et P.H. McBreen, *J. Am. Chem. Soc.* **116**, 5965 (1994).

Martel, R.; McBreen, P. J. Chem. Phys. 1997, 107, 8619.

McCulloh K. E., *J. Chem. Phys.* **59**, 4250 (1973).

McDiarmid R. et J.P. Doering, *J. Chem. Phys.* **80**, 648 (1984).

Michaud M. et L. Sanche, *J. Electron. Spectrosc. Relat. Phenom.* **51**, 237 (1990).

Michaud M., P. Cloutier, et L. Sanche, *Rev. Sci. Instrum.* **66**, 2661 (1995).

Monahan K. M. et W. C. Walker, *J. Chem. Phys.* **61**, 3886 (1974).

Nakatsuji H., *Chem. Phys.* **75**, 425 (1983).

Olsen C. et P.A. Rowntree, *J. Chem. Phys.* **108**, 3750 (1998).

Orient O.J. et S.K. Srivastava, *Chem. Phys. Letters* **96**, 681 (1983)

Padial N., G. Csanak, B. V. McKoy, et P. W. Langhoff, *Phys. Rev. A* **23**, 218 (1981).

Pylant E.D., M.J. Hubbard, et J.M. White, *J. Phys. Chem.* **100**, 15890 (1996).

Rapp D. et D.D. Briglia, *J. Chem. Phys.* **43**, 1480 (1965).

Reineck I., C. Nohre, R Maripuu, P. Lodin, S. H. Al-Shamma, H Veenhuizen, L Karlsson, et K. Siegbahn, *Chem. Phys.* **78**, 311 (1983).

Robin M.B., *Higher Excited States of Polyatomic Molecules*, Vol. I, (Academic Press, New York, 1974).

Robin M.B., *Higher Excited States of Polyatomic Molecules*, Vol. II, (Academic Press, New York, 1975).

Robin M.B., *Higher Excited States of Polyatomic Molecules*, Vol. III, (Academic Press, New York, 1985).

Rowntree P., L. Parenteau, et L. Sanche, *J. Phys. Chem.* **95**, 4902 (1991).

Sanche L., *Interaction of Low-Energy Electrons with Atomic and Molecular Solids, Scanning Microscopy* **9**, 619 (1995).

Sanche L., *J. Phys. B* **23**, 1597 (1990).

Sanche L., *J. Chem. Phys.* **71**, 4860 (1979).

Sanche L. et M. Michaud, *Phys. Rev. B* **30**, 6078 (1984).

Sanche L. et L. Parenteau, *Phys. ReV. Lett.* **59**, 136 (1987).

Schulz G. J., *Phys. Rev.* **128**, 178 (1962).

Schulz G.J. et D. Spence, *Phys. Rev. Lett.* **52** (1969).

Scoggins T. B., H. Ihm, Y. M. Sun, et J. M. White, *J. Phys. Chem. B* **103**, 6791 (1999).

Spielfiedel A., N. Feautrier, C. Cossart-Magos, G. Chambeau, P. Rosmus, H.-J. Werner, et P. Botschwina, *J. Chem. Phys.* **97**, 8382 (1992).

Spotheim-Maurizot M., J. Franchet, R. Sabattier, et M. Charlier, *Int. J. Radiat. Biol.* **59**, 1313 (1991).

Srivastava S.K. et O.J. Orient, *Phys. Rev. A* **27**, 1210 (1983).

Stamatovic A. et G.J. Schulz, *Phys. Rev. A* **7**, 589 (1973).

Swiderek P. et H. Winterling, *Chem. Phys.* **229**, 295 (1998).

Swiderek P., M. C. Deschamps, M. Michaud, et L. Sanche, *J. Phys. Chem. B* **107**, 563 (2003).

Swiderek P., M. Michaud, et L. Sanche, *J. Chem. Phys.* **98**, 8397 (1993).

Swiderek P., M. Michaud, et L. Sanche, *J. Chem. Phys.* **103**, 8424 (1995).

Tanaka H. et M. Inokuti, *Adv. At. Mol. Opt. Phys.* **43**, 1 (2000).

Tian C., C.R. Vidal, *Phys. Rev. A* **58**, 3783 (1998).

Tronc M., R. Azria, Y. Le Coat, P. Cloutier, et L. Sanche, *Chem. Phys.* **254**, 69 (2000).

Ulbricht J., *Grundlagen der Synthese von Polymeren*, Hüthig & Wepf, Basel, 1992.

Winter N. W., C. F. Bender, et W. A. Goddard III, *Chem. Phys. Lett.* **20**, 489 (1973).

Winterling H., H. Haberkern, et P. Swiderek, *Phys. Chem. Chem. Phys.* **3**, 4592 (2001).